Measurement and modeling of neutral, radical, and ion densities in H2-N2-Ar plasmas

M. Sode, W. Jacob, T. Schwarz-Selinger, and H. Kersten

Citation: Journal of Applied Physics **117**, 083303 (2015); doi: 10.1063/1.4913623
View online: http://dx.doi.org/10.1063/1.4913623
View Table of Contents: http://scitation.aip.org/content/aip/journal/jap/117/8?ver=pdfcov
Published by the AIP Publishing

Measurement and modeling of neutral, radical, and ion densities in H_2-N_2-Ar plasmas

M. Sode,[1,a)] W. Jacob,[1] T. Schwarz-Selinger,[1] and H. Kersten[2]
[1]*Max-Planck-Institut für Plasmaphysik, Boltzmannstraße 2, D-85748 Garching, Germany*
[2]*Institute for Experimental and Applied Physics, Christian-Albrechts-Universität zu Kiel, Leibnizstraße 11-19, D-24098 Kiel, Germany*

(Received 12 December 2014; accepted 15 February 2015; published online 27 February 2015)

A comprehensive experimental investigation of absolute ion and neutral species densities in an inductively coupled H_2-N_2-Ar plasma was carried out. Additionally, the radical and ion densities were calculated using a zero-dimensional rate equation model. The H_2-N_2-Ar plasma was studied at a pressure of 1.5 Pa and an *rf* power of 200 W. The N_2 partial pressure fraction was varied between $f_{N_2} = 0\%$ and 56% by a simultaneous reduction of the H_2 partial pressure fraction. The Ar partial pressure fraction was held constant at about 1%. NH_3 was found to be produced almost exclusively on the surfaces of the chamber wall. NH_3 contributes up to 12% to the background gas. To calculate the radical densities with the rate equation model, it is necessary to know the corresponding wall loss times t_{wrad} of the radicals. t_{wrad} was determined by the temporal decay of radical densities in the afterglow with ionization threshold mass spectrometry during pulsed operation and based on these experimental data the absolute densities of the radical species were calculated and compared to measurement results. Ion densities were determined using a plasma monitor (mass and energy resolved mass spectrometer). H_3^+ is the dominant ion in the range of $0.0 \leq f_{N_2} < 3.4\%$. For $3.4 < f_{N_2} < 40\%$, NH_3^+ and NH_4^+ are the most abundant ions and agree with each other within the experimental uncertainty. For $f_{N_2} = 56\%$, N_2H^+ is the dominant ion, while NH_3^+ and NH_4^+ have only a slightly lower density. Ion species with densities in the range between 0.5% and 10% of $n_{i,tot}$ are H_2^+, ArH^+, and NH_2^+. Ion species with densities less than 0.5% of $n_{i,tot}$ are H^+, Ar^+, N^+, and NH^+. Our model describes the measured ion densities of the H_2-N_2-Ar plasma reasonably well. The ion chemistry, i.e., the production and loss processes of the ions and radicals, is discussed in detail. The main features, i.e., the qualitative abundance of the ion species and the ion density dependence on the N_2 partial pressure fraction, are well reproduced by the model.
[http://dx.doi.org/10.1063/1.4913623]

I. INTRODUCTION

Plasmas containing H_2-N_2 are extensively applied for thin film growth and material processing on the nanometer scale.[1–3] For example, thin films of silicon nitride which are fabricated by plasma-enhanced chemical vapor deposition (PECVD) in the semiconductor industry are used as passivation layers[4] and in the photovoltaic industry.[3,5] For the etching of organic low-k layers, hydrofluorocarbons are replaced by H_2-N_2 due to economic and ecological reasons.[6,7] Other applications of H_2-N_2 plasmas are nitriding,[8,9] the plasma-enhanced atomic layer deposition of TaN and TiN thin films,[8,10] the etching of organic low dielectric constant (low-k) films,[6,8,11] and the chemical synthesis of ammonia.[8,12,13] The latter is also of interest in nuclear fusion research where N_2 is puffed into the plasma edge of the hydrogen plasma to reduce the local heat load of the so-called divertor region.[14–19] Argon addition to H_2-N_2 plasmas is applied in fusion plasmas[16,17] as well as for industrial nitriding treatments of ferrous and nonferrous materials for improving the mechanical properties or corrosion resistance.[20,21] In many of these plasmas, the dominant plasma-surface-interaction processes are driven by radical species or ions or a synergistic interaction, respectively, between them. Hence, a quantitative determination of ion and radical densities is a prerequisite for an improved understanding of plasma-surface-interactions in those reactive plasmas.

In two preceding publications,[22,23] a comprehensive investigation of a H_2-Ar plasma was presented. The densities of the gas species, the radical species H, the electrons, and the ion species as well as the temperature of the gas were determined experimentally.[22] Furthermore, by a rate equation model, the ion densities, the atomic hydrogen density, and the electron temperature were studied theoretically.[23] One of the main results of Refs. 22 and 23, namely, the ion species distribution, is in reasonable agreement with recent publications of Fox-Lyon *et al.*[24] and Jimenez-Redondo *et al.*[25] studying H_2-Ar plasmas at comparable pressures. The H_2-Ar plasma can be considered as a model system with a much lower complex plasma chemistry than a H_2-N_2-Ar plasma. For this model system, the experimental methods as well as the rate equation model were benchmarked for our experimental setup and will here be applied for the more complex H_2-N_2-Ar plasma.

In low temperature H_2-N_2-Ar plasmas, H_2, N_2, Ar, and NH_3—NH_3 is produced in the plasma—are the stable background gas species. H, N, NH, and NH_2 are the relevant radical species. The primary ions which are produced by

a)Electronic mail: maik.sode@ipp.mpg.de

electron-induced ionization of neutrals are H_2^+, N_2^+, Ar^+, and NH_3^+ as well as H^+, N^+, NH^+, and NH_2^+. In addition, the secondary ions H_3^+, NH_4^+, N_2H^+, and ArH^+, which are solely produced by ion-molecule reactions, appear. Furthermore, N_2H_x neutrals and their ions can also appear (see, e.g., Ref. 26), but due to their extremely low density these species are not considered in the present work.

A similar extensive study of H_2-N_2 plasmas as in the present work was carried out by Carrasco *et al.*[3,27,28] in a DC hollow cathode discharge with comparable plasma conditions. Carrasco *et al.* presented experimental and modeling results for densities of ionic, electron, radical, and gas species. The basic mechanisms leading to the observed neutral and ion distributions, as well as their relative importance in the studied pressure range, were identified and discussed. Jang and Lee[29] previously examined a few aspects in an inductively coupled H_2-N_2 plasma by measuring n_e, T_e, and ion signal intensities. In addition, there exists a variety of studies about H_2-N_2 plasmas in which the densities of background gas species,[13,20,30–33] radicals,[7,8,20,32,34] electrons,[34,35] and ion signals[7,36] as well as the surface loss probability of H and N (see Ref. 7) were reported. Other studies have calculated the most important species densities using rate equation models.[37–40] However, these studies rarely compared calculated results with experimental data. Therefore, an assessment of rate equation models with experimental data is only partially given. Argon admixtures to hydrogen and nitrogen containing plasmas were examined in the studies of Refs. 20, 26, 31, 35, and 36.

In H_2-N_2 plasmas, NH_3 is commonly produced by plasma chemical reactions. The formation of NH_3 is quantitatively not yet fully understood, but it is generally assumed that NH_3 is produced mainly by surface reactions at the plasma surrounding wall.[3,30,38] Atomic nitrogen and hydrogen originating from electron-impact dissociation in the plasma are expected to synthesize on the surface resulting in NH_x ($x = 1, 2$) and finally in NH_3. Surface reaction models describing the production of NH_3 are available from Gordiets *et al.*[37,38] and Carrasco *et al.*[3,28]

In the present work, a comprehensive investigation of an inductively coupled H_2-N_2-Ar plasma at 1.5 Pa is performed. The total pressure of 1.5 Pa is kept constant, while the N_2 partial pressure fraction f_{N_2} is varied between 0% and 56%, whereas the H_2 partial pressure fraction f_{H_2} is reduced correspondingly. The Ar partial pressure fraction is fixed at 1%. Densities n_j of background gas species, wall loss times t_{wrad} and densities n_{rad} of radicals, the gas temperature T_g, the electron temperature T_e, the electron density n_e, and ion densities n_i will be presented. The same measurement methods and rate equation model as in a preceding study of a H_2-Ar plasma[22,23] are applied here. The determined ion densities will be discussed and compared with the model results. Finally, the ion chemistry, i.e., the dominant plasma-chemical reactions in the plasma, will be specified based on the model results.

II. EXPERIMENT

A. Plasma chamber setup

In the following, we briefly present the experimental methods. A detailed description can be found in Ref. 22. The experimental setup consists of a cylindrical stainless steel plasma chamber. The discharge is generated by a planar coil with 5 turns driven by a radio frequency (*rf*) generator operating at 13.56 MHz (Dressler Cesar 136). The coil is separated from vacuum by a quartz dome.[41] The top part of the dome acts as the dielectric window for the *rf* power. The outer diameter d_{el} of the quartz window and the upper stainless steel electrode is $d_{el} = 2r_{el} = 131$ mm, where r_{el} is the corresponding radius. The distance l_{el} between the stainless steel electrode and dielectric quartz window is $l_{el} = 60$ mm. The plasma is mainly generated in the assumed cylinder with the volume $V = \pi r_{el}^2 l_{el} = 0.80$ l between the electrode and the quartz window although at r_{el} there is no radial side wall between the stainless steel electrode and dielectric window. The stainless steel vacuum chamber has a radius of $r_{ch} = 125$ mm and a total height of $l_{ch} = 360$ mm.

In this work, H_2-N_2-Ar low-temperature plasmas with variable N_2 content are investigated. The total pressure of 1.5 Pa is kept constant, while the N_2 partial pressure fraction f_{N_2} is increased on expense of f_{H_2}. A constant *rf* power of 200 W is used in all experiments. A butterfly valve in front of the turbo molecular pump allows to throttle the pumping speed. All experiments were conducted with a fixed butterfly position so that the residence time of the species was constant ($t_{H_2} = 0.19$ s, $t_{N_2} = 0.77$ s, $t_{Ar} = 31$ s). The incoming gas flows were adjusted with mass-flow controllers. For the chosen butterfly position, the required gas flows to achieve the working pressure of 1.5 Pa are $\Phi_{max,H_2} = 79.5$ sccm in case of pure H_2 and $\Phi_{max,N_2} = 20$ sccm for pure N_2. For different gas mixtures, Φ_{N_2} is increased from 0 to 20 sccm, whereas Φ_{H_2} is lowered from 79.5 to 24 sccm. For all measurements, a constant Ar gas flow of $\Phi_{Ar} = 0.5$ sccm is used. The working pressure prior to plasma ignition of $p = 1.5$ Pa is used for all considered plasma conditions shown here.

B. Partial pressures

Previous investigations by mass spectrometry have shown that for the applied experimental conditions the flux ratios of the working gases are not identical to the partial pressure fractions.[22] Therefore, the actual partial pressure fractions f_j for a gas species j used in the experiment were determined with a quadrupole mass spectrometer. A differentially pumped molecular-beam mass spectrometer "MBMS" (QMG 422, Pfeiffer Vacuum) with cross-beam ion source was used to measure the actual partial pressures in the gas mixtures (see also Ref. 22 for details). Particles are sampled through a capillary at the outer diameter of the vessel in the central plane. The partial pressure fraction is defined as $f_j = p_j/p_{tot}$, where p_j and p_{tot} are the partial and total pressures measured with the MBMS, respectively. The mass spectrometer chamber is equipped with a stainless steel shutter behind the capillary to allow distinguishing the isotropic background signal inside the chamber from the signal due to the molecular beam that is formed by the capillary. The particle density in this molecular beam is proportional to the particle density in the vessel.[42] Therefore, the beam signals are a good measure for the particle densities and accordingly partial pressures. The beam component was obtained

by subtracting the signal with closed shutter from the signal with opened shutter. The beam-to-background ratio R was measured and yields for H_2 $R_{H_2} = 1.5 \pm 0.1$, for N_2 $R_{N_2} = 4.4 \pm 0.3$, for Ar $R_{Ar} = 5.0 \pm 0.3$, and for NH_3 $R_{NH_3} = 3.8 \pm 0.3$. The values are independent on pressure in the considered range up to 1.5 Pa.

In the following, the procedure for determining the partial pressure fraction is described. A certain flow of a pure gas corresponds to a certain pressure in the main chamber for the fixed butterfly position. This pressure corresponds to the beam component measured with the mass spectrometer. The beam components of the mass spectrometer signals for the pure gases were calibrated against the pressure in the main chamber measured with a capacitive manometer. This calibration was made for the full partial pressure range applied in the experiments. Such calibrated mass spectrometer was in the following used to measure the partial pressures of the gas species in the gas mixtures.

C. Gas temperature and actinometry

Optical emission spectroscopy (OES) was applied to measure the gas temperature and the dissociation degree of hydrogen as described in Ref. 22. The used spectrometer is a Czerny-Turner spectrograph (Acton SpectraPro 275) with a focal length of 275 mm. The experiments were conducted with a 1800 lines/mm grating, which has a resolution of 0.15 nm at $\lambda = 600$ nm.

The H_2 gas temperature T_g is derived from the rotational temperature T_{rot} of the H_2 molecule. T_{rot} of the hydrogen molecule is derived from the rotational lines Q_1–Q_3 of the Q-branch of the H_2 Fulcher-α diagonal band $(v' = v'' = 2)$ with experimental uncertainty of 50 K.[22] T_{rot} was experimentally determined for all considered N_2 partial pressures. A mean value of $T_{rot} = 460 \pm 50$ K is obtained. We want to note that in a former study[43] the rotational temperature of molecular nitrogen was evaluated from the spectrum of the transition $v' = 0 \rightarrow v'' = 2$ of the second positive system $(C^3\Pi_u \rightarrow B^3\Pi_g)$ of N_2. T_{rot} from H_2 and N_2 were in very good agreement with each other within the experimental uncertainty (see Ref. 43). T_{rot} is, therefore, taken as an estimate of the gas temperature T_g and is applied to calculate the gas densities according to an ideal gas law

$$n_j = f_j \frac{p}{k_B T_g}, \tag{1}$$

for the background gas j with the partial pressure fraction f_j (k_B—Boltzmann constant).

The dissociation degree of hydrogen is here defined as n_H/n_{H_2} with n_H being the atomic hydrogen density and n_{H_2} the molecular hydrogen density in the plasma. n_H/n_{H_2} was determined by actinometry using the ratio of the H_β/Ar_{750} lines as described in Ref. 44. The experimental uncertainty for the dissociation degree is 24% (see Ref. 44).

D. Electron temperature and density

The electron energy distribution function (EEDF), the electron temperature T_e, and the electron density n_e were determined by a single-tip Langmuir probe system.[22] The probe consists of a single cylindrical tungsten tip 4 mm in length and 40 μm in diameter. I-V curves are acquired with the control and measuring unit PlasmaMeter.[45,46] T_e is calculated by the potential difference $\Delta V = V_{pl} - V_{fl}$ method,[22] where V_{pl} and V_{fl} denote the plasma and the floating potential, respectively, and n_e is calculated by integrating the EEDF.[22] The Langmuir probe measurements were performed in the axial center of the plasma ($r = 0$ mm), 20 mm above the quartz window.

E. Ion densities

A combined energy and mass analyzer (Pfeiffer plasma process monitor PPM 422, Inficon AG Balzers)—in the following designated as plasma monitor (PM)—is incorporated into the upper, grounded electrode. The plasma monitor is twofold differentially pumped resulting in a background pressure of the order of 10^{-6} Pa for a working pressure of 1 Pa in the plasma chamber. Particles are sampled through two aligned orifices (100 and 500 μm in diameter, respectively) at the center of the electrode. The plasma monitor consists of an einzel lens (EL), an electron-impact ionizer (IZ) to detect neutrals, a cylindrical-mirror energy analyzer (CMA), a quadrupole mass filter (QMS), and a secondary electron multiplier (SEM) as particle detector arranged in series. There is also a Faraday cup as particle detector installed, but because of better dynamic range the SEM was used in this study. A discriminator voltage V_{PM} accelerates or decelerates incoming ions to a constant pass energy of 15 eV in the energy filter. The plasma monitor measures either in the so called "mass mode" at a fixed discriminator voltage V_{PM} or in the so called "energy mode" at a fixed mass to charge ratio M_i of a species i (here only singly charged ions are assumed).

A calibration procedure was applied to derive absolute ion densities from mass-resolved signal intensities of the PM.[22] The calibration procedure considers the energy-dependent (T_{ed}) and mass-dependent (T_{md}) transmission of the plasma monitor. In our case, the ion energy distributions (IEDs) for one plasma condition are similar in position and shape. In first order approximation, only the heights $H_{PM,i}$ of the IEDs vary with individual ion species i. As it was shown in Ref. 22, it is possible to convert $H_{PM,i}$ into relative ion fluxes $j_{PM,i,rel}$:

$$j_{PM,i,rel} \propto 1/T_{md}(M_i) \times H_{PM,i}, \tag{2}$$

(M_i—mass of ion species i). In Ref. 22, a Faraday cup was used as detector and, therefore, T_{md} was only determined by the quadrupole. Here, we have to take into account also the mass-dependent sensitivity of the SEM. However, analyzing the mass-dependent transmission of the SEM has shown that T_{md} agrees between SEM and Faraday cup except for the light ions $i = H^+, H_2^+, H_3^+$. Furthermore, for these light ions the shapes, i.e., the energy of the maximum of the ion energy distribution, differ slightly from those of the other ion species. Therefore, for $i = H^+, H_2^+, H_3^+$ correction factors are determined accounting for the deviation in the maxima of the ion energy distributions and the difference between measurements with SEM and Faraday cup.

The conversion from relative fluxes into relative ion densities $n_{PM,i,rel}$ is based on a sheath and density profile model[22]

$$n_{PM,i,rel} = \sqrt{M_i}/h_{l,i} \times j_{PM,i,rel}, \quad (3)$$

where $h_{l,i}$ is the ion density ratio between sheath edge and plasma bulk (see Sec. III C). To convert these relative fluxes to absolute fluxes, the electron density n_e measured with the Langmuir probe is used. The calibration factor C_{calib} which converts relative ion densities into absolute ion densities is obtained from

$$C_{calib} = \frac{n_e}{\sum_i n_{PM,i,rel}}. \quad (4)$$

n_e is set equal to the total ion density due to quasi neutrality.

The reproducibility of the plasma monitor was checked by repeating the whole set of H_2-N_2-Ar measurements with the same experimental settings on two different days. The standard deviation of the relative changes of the individual plasma monitor signal heights determined from this comparison was 15%.

F. Radical wall loss times

The radical wall loss time which is an important model input parameter is determined by monitoring the radical density in the temporal afterglow of the plasma with ionization threshold mass spectroscopy (ITMS).[47–53] This technique takes advantage of the fact that the threshold energy for direct ionization of a radical, e.g., $e^- + N \rightarrow N^+ + 2e^-$ is lower than the threshold energy for the corresponding dissociative ionization of the mother molecules leading to the same ion, e.g., $e^- + N_2 \rightarrow N^+ + N + 2e^-$. The electron energy E_{cath} in the ionizer is set between these two thresholds. This allows discriminating the radical signal from the signal of stable neutrals, which are usually much more abundant. The experimental technique applied here is described in detail in Ref. 43. For the measurement of relative radical densities, the plasma monitor in the neutral modus is used operating with a fixed electron energy E_{cath}. For atomic nitrogen (mass channel 14 amu/e), a E_{cath} of 18 eV is used. The determination of the used E_{cath} for N is explained in detail in Ref. 43. For the radicals hydrogen H on mass channel 1 amu/e (deuterium D on 2 amu/e), NH on mass channel 15 amu/e (ND on 16 amu/e), and NH_2 on mass channel 16 amu/e (ND_2 on 18 amu/e), the electron energies $E_{cath}(H^+) = 15$ eV, $E_{cath}(NH^+) = 16$ eV, and $E_{cath}(NH_2^+) = 14$ eV are used, respectively.[54]

For radicals, the density in the afterglow and, hence, the signal intensity collected during one single decay is low. To increase counting statistics, the plasma is operated in pulsed mode and signals are collected with a multi-channel scaler card. The signal pulses (measuring events) of the secondary electron multiplier of our mass spectrometer are detected by multi-channel scaler cards (MCS, 65536 channels, Ortec). The pulsed plasma is operated with a power-on phase (P_{on}) with a duration of t_{on} and a power-off phase (P_{off}) with a duration of t_{off}. A pulse generator is used which switches on and off the *rf* generator and provides the trigger signal for the mass spectrometer measurements. For further details, see Ref. 43. The signal S is computed from $S = N/(m_{cycle} \times t_{dwell})$ (N—counting events, m_{cycle}—number of pulses, $t_{dwell} = 0.05$ ms—dwell time for N) and has the unit counts per second (cps).

III. MODEL

We apply a zero-dimensional rate equation model to calculate the ion densities n_i, the radical densities n_{rad}, and the electron temperature T_e in these H_2-N_2-Ar plasmas. The model is described in detail in Ref. 23, where it was applied to H_2-Ar plasmas. The model takes into account densities of electrons, positive ions, radicals, and the stable background gas species. Furthermore, for Ar, N_2, and N excited levels are included. An overview of the considered species in the H_2-N_2-Ar plasma is given in Table I. For the particle balance, collisions in the volume and losses to the plasma-surrounding walls are taken into account.

The main input parameters for the model are all the required collision rate coefficients. The remaining input parameters are experimentally obtained quantities, namely, the electron density n_e, the gas temperature T_g, the total pressure p, the radical wall loss times, the partial pressure fractions f_j, and the geometry of the discharge vessel. The model output values are n_i, n_{rad}, and T_e. The densities are obtained by solving the rate equation system using the online available solver "Kinetic PreProcessor"[55,56] (*KPP*). In *KPP*, the rate equation system is solved using the Rosenbrock algorithm, which is based on semi-implicit Runge-Kutta methods with adaptive stepsize. To achieve self-consistency, the quasi-neutrality has to be fulfilled which is imposed externally as an additional boundary condition. The calculated electron temperature T_e^c is varied to achieve the quasi-neutrality $n_e = \sum_i n_i$, where i is the ion species. T_e^c is accepted if the condition $0.98 \leq (\sum_i n_i)/n_e \leq 1.02$ is satisfied.

A. Model assumptions

The model is based on the following assumptions and simplifications:

(1) The model is zero-dimensional.
(2) The loss of particles to the surrounding walls is volume averaged. The model predicts species densities in the plasma center.
(3) The calculated densities are determined for the steady state.

TABLE I. Overview of the considered species in the H_2-N_2-Ar plasmas.

Background gas	H_2, N_2, Ar, NH_3
Radicals	H, N, NH, NH_2
Electrons	e^-
Ions	H^+, H_2^+, H_3^+, N^+, NH^+, NH_2^+, NH_3^+, NH_4^+, N_2^+, N_2H^+, Ar^+, ArH^+
Excited species	$N_2(A)$, $N_2(B)$, $N_2(C)$, $N_2(a')$, N(*D*), N(*P*), Ar_{meta}, Ar_r, Ar(2*p*)

(4) The temperature of the neutrals and ion species is described by one gas temperature T_g, which is set equal to the measured rotational temperature T_{rot} of the H_2 molecules ($T_{rot} = 460$ K, see Sec. II C).
(5) The following reaction types are taken into account: electron collisions with the background gas, heavy-particle (i.e., ions) collisions with the background gas (see Sec. III B).
(6) Wall loss for radicals (see Sec. IV) and for ions (see Sec. III C) is taken into account.
(7) The following reaction types occurring in the plasma volume are not considered due to very low reaction rates: neutral heavy-particle collisions involving radicals, three-body interactions, and electron-ion recombination.
(8) The following excited species are taken into account: excited levels of Ar, N_2, and N (see Sec. III D).
(9) The following species are not taken into account: negative ions (due to very low concentrations with respect to the electron density[37,57]) and vibrationally excited molecular levels.
(10) The density of NH_3 is a model input parameter and is taken from the measurement. In this work, no surface model for the description of the surface processes yielding NH_3 is considered.
(11) In the model, the densities of the background gas species are not affected by the plasma and, therefore, kept constant for the discharge. This is based on the fact that the degree of dissociation (<10%) and also the degree of ionization ($\approx 10^{-4}$) are very low. One indication that this assumption is fulfilled is that the measured pressure after plasma ignition does not significantly change (<4%). The change of <4% is attributed to NH_3 production. As input parameters, the measured partial pressure fractions f_j during plasma operation are used.

B. Electron and ion-molecule collisions

The rate coefficients K_k for electron collisions are calculated from the corresponding cross sections σ_k by averaging the product $\sigma_k \times v_e$ (v_e—electron velocity) over a Maxwellian electron energy distribution function (for details, see Ref. 23). The values for the considered electron collisions are compiled in Table II. From here on the rate coefficients K_k will be labeled according to the index k for the corresponding reaction listed in Tables II–VIII. Yoon *et al.*[58] and Itikawa[61] compiled a collection of recommended values of cross sections for electron collisions with hydrogen and nitrogen molecules, respectively. We consider these data as the presently most reliable data set. Shah *et al.*[59] and Wetzel *et al.*[60] measured electron ionization cross sections and compared their results to the existing literature data. Their values agree with published data within 15%. For the ionization cross sections of NH_3, there exist only few publications (Tarnovsky *et al.*[63] and Märk *et al.*[64]), for NH_2 and NH there is only one publication (Tarnovsky *et al.*[63]). The dissociation of NH_3 leads to 3 products (reactions 1.19–1.21 in Table II). The corresponding dissociation cross sections are taken from Yousfi and Benabdessadok.[65] The dissociation cross sections for NH_2 and NH are taken from van Laer *et al.*[11] The rate coefficient of reaction 1.25 whose reaction is of minor importance is directly taken from Ref. 57.

TABLE II. Reaction set with rate coefficients K for electron collisions with index k (T_e in eV).

k	Reaction	$K(\mathrm{m^3 s^{-1}})$	Reference
1.1	$e^- + H_2 \rightarrow 2H + e^-$	$8.4 \times 10^{-14} T_e^{-0.45} \times e^{-11.18/T_e}$	σ from Ref. 58
1.2	$e^- + H \rightarrow H^+ + 2e^-$	$1.1 \times 10^{-14} T_e^{0.29} \times e^{-15.28/T_e}$	σ from Ref. 59
1.3	$e^- + H_2 \rightarrow H_2^+ + 2e^-$	$2.3 \times 10^{-14} T_e^{0.19} \times e^{-17.87/T_e}$	σ from Ref. 58
1.4	$e^- + H_2 \rightarrow H^+ + H + 2e^-$	$9.4 \times 10^{-16} T_e^{0.45} \times e^{-29.94/T_e}$	σ from Ref. 58
1.5	$e^- + Ar \rightarrow Ar^+ + 2e^-$	$3.7 \times 10^{-14} T_e^{0.38} \times e^{-17.64/T_e}$	σ from Ref. 60
1.6	$e^- + N_2 \rightarrow N + N(D) + e^-$	$2.4 \times 10^{-14} T_e^{0.27} \times e^{-15.53/T_e}$	σ from Ref. 61
1.7	$e^- + N \rightarrow N^+ + 2e^-$	$9.3 \times 10^{-15} T_e^{0.56} \times e^{-16.66/T_e}$	σ from Ref. 62
1.8	$e^- + N_2 \rightarrow N_2^+ + 2e^-$	$1.3 \times 10^{-14} T_e^{0.56} \times e^{-17.07/T_e}$	σ from Ref. 61
1.9	$e^- + N_2 \rightarrow N^+ + N + 2e^-$	$2.9 \times 10^{-15} T_e^{0.72} \times e^{-29.71/T_e}$	σ from Ref. 61
1.10	$e^- + NH_3 \rightarrow NH_3^+ + 2e^-$	$1.5 \times 10^{-14} T_e^{0.40} \times e^{-13.61/T_e}$	σ from Ref. 63
1.11	$e^- + NH_3 \rightarrow NH_2^+ + H + 2e^-$	$1.6 \times 10^{-14} T_e^{0.34} \times e^{-15.41/T_e}$	σ from Ref. 63
1.12	$e^- + NH_3 \rightarrow NH^+ + 2H + 2e^-$	$5.4 \times 10^{-16} T_e^{0.37} \times e^{-26.06/T_e}$	σ from Ref. 63
1.13	$e^- + NH_3 \rightarrow N^+ + H + H_2 + 2e^-$	$8.8 \times 10^{-17} T_e^{0.59} \times e^{-29.00/T_e}$	σ from Ref. 64
1.14	$e^- + NH_3 \rightarrow H^+ + NH_2 + 2e^-$	$1.3 \times 10^{-16} T_e^{0.47} \times e^{-28.55/T_e}$	σ from Ref. 64
1.15	$e^- + NH_2 \rightarrow NH_2^+ + 2e^-$	$1.3 \times 10^{-14} T_e^{0.50} \times e^{-12.40/T_e}$	σ from Ref. 63
1.16	$e^- + NH_2 \rightarrow NH^+ + H + 2e^-$	$2.2 \times 10^{-14} T_e^{0.21} \times e^{-17.97/T_e}$	σ from Ref. 63
1.17	$e^- + NH \rightarrow NH^+ + 2e^-$	$2.1 \times 10^{-14} T_e^{0.37} \times e^{-15.49/T_e}$	σ from Ref. 63
1.18	$e^- + NH \rightarrow N^+ + H + 2e^-$	$7.6 \times 10^{-15} T_e^{0.29} \times e^{-16.82/T_e}$	σ from Ref. 63
1.19	$e^- + NH_3 \rightarrow NH_2 + H + e^-$	$4.2 \times 10^{-14} T_e^{-0.19} \times e^{-7.59/T_e}$	σ from Ref. 65
1.20	$e^- + NH_3 \rightarrow NH + 2H + e^-$	$1.3 \times 10^{-14} T_e^{0.38} \times e^{-11.06/T_e}$	σ from Ref. 65
1.21	$e^- + NH_3 \rightarrow NH + H_2 + e^-$	$4.1 \times 10^{-14} T_e^{-0.26} \times e^{-4.84/T_e}$	σ from Ref. 65
1.22	$e^- + NH_2 \rightarrow NH + H + e^-$	$4.5 \times 10^{-14} T_e^{-0.22} \times e^{-7.61/T_e}$	σ from Ref. 11
1.23	$e^- + NH_2 \rightarrow N + H_2 + e^-$	$1.5 \times 10^{-14} T_e^{0.38} \times e^{-11.44/T_e}$	σ from Ref. 11
1.24	$e^- + NH \rightarrow N + H + e^-$	$4.7 \times 10^{-14} T_e^{-0.22} \times e^{-7.69/T_e}$	σ from Ref. 11
1.25	$e^- + H_2^+ \rightarrow H^+ + H + e^-$	$1.5 \times 10^{-13} \times e^{-1.97/T_e}$	K from Ref. 57

TABLE III. Reaction set for ion-molecule reactions k.

k	Reaction	$K(\mathrm{m^3 s^{-1}})$	Reference
2.1	$H_2^+ + H_2 \rightarrow H_3^+ + H$	2.0×10^{-15}	66
2.2	$ArH^+ + H_2 \rightarrow H_3^+ + Ar$	6.3×10^{-16}	66
2.3	$H_2^+ + Ar \rightarrow ArH^+ + H$	2.1×10^{-15}	66
2.4	$H_2^+ + Ar \rightarrow Ar^+ + H_2$	2.0×10^{-16}	66
2.5	$H_3^+ + Ar \rightarrow ArH^+ + H_2$	3.7×10^{-16}	66
2.6	$Ar^+ + H_2 \rightarrow ArH^+ + H$	8.7×10^{-16}	66
2.7	$Ar^+ + H_2 \rightarrow H_2^+ + Ar$	1.8×10^{-17}	66
2.8	$N^+ + N_2 \rightarrow N_2^+ + N$	2.0×10^{-17}	67
2.9	$N_2^+ + N \rightarrow N^+ + N_2$	1.0×10^{-17}	66
2.10	$Ar^+ + N_2 \rightarrow N_2^+ + Ar$	1.1×10^{-17}	66
2.11	$N_2^+ + Ar \rightarrow Ar^+ + N_2$	2.0×10^{-19}	66
2.12	$N_2^+ + H_2 \rightarrow N_2H^+ + H$	2.0×10^{-15}	66
2.13	$H_2^+ + N_2 \rightarrow N_2H^+ + H$	2.0×10^{-15}	66
2.14	$H_3^+ + N_2 \rightarrow N_2H^+ + H_2$	1.9×10^{-15}	66
2.15	$H_3^+ + NH_3 \rightarrow NH_4^+ + H_2$	4.4×10^{-15}	66
2.16	$N^+ + H_2 \rightarrow NH^+ + H$	5.0×10^{-16}	66
2.17	$NH_2^+ + H_2 \rightarrow NH_3^+ + H$	2.0×10^{-16}	66
2.18	$H_2^+ + N \rightarrow N^+ + H_2$	5.0×10^{-16}	26
2.19	$Ar^+ + NH_2 \rightarrow NH^+ + H + Ar$	5.5×10^{-17}	26
2.20	$H^+ + NH_3 \rightarrow NH_3^+ + H$	5.2×10^{-15}	66
2.21	$H_2^+ + NH_3 \rightarrow NH_3^+ + H_2$	5.7×10^{-15}	66
2.22	$H_3^+ + N \rightarrow NH^+ + H_2$	2.6×10^{-16}	66
2.23	$H_3^+ + N \rightarrow NH_2^+ + H$	3.9×10^{-16}	66
2.24	$N^+ + NH_3 \rightarrow NH_2^+ + NH$	4.7×10^{-16}	66
2.25	$N^+ + NH_3 \rightarrow NH_3^+ + N$	1.7×10^{-15}	66
2.26	$N^+ + NH_3 \rightarrow N_2H^+ + H_2$	2.1×10^{-16}	66
2.27	$NH^+ + H_2 \rightarrow H_3^+ + N$	1.8×10^{-16}	66
2.28	$NH^+ + H_2 \rightarrow NH_2^+ + H$	1.0×10^{-15}	66
2.29	$NH^+ + NH_3 \rightarrow NH_3^+ + NH$	1.8×10^{-15}	66
2.30	$NH^+ + NH_3 \rightarrow NH_4^+ + N$	6.0×10^{-16}	66
2.31	$NH^+ + N_2 \rightarrow N_2H^+ + N$	6.5×10^{-16}	66
2.32	$NH_2^+ + NH_3 \rightarrow NH_3^+ + NH_2$	1.2×10^{-15}	66
2.33	$NH_2^+ + NH_3 \rightarrow NH_4^+ + NH$	1.2×10^{-15}	66
2.34	$NH_3^+ + H_2 \rightarrow NH_4^+ + H$	4.4×10^{-19}	66
2.35	$NH_3^+ + NH_3 \rightarrow NH_4^+ + NH_2$	2.1×10^{-15}	66
2.36	$N_2^+ + NH_3 \rightarrow NH_3^+ + N_2$	2.0×10^{-15}	66
2.37	$N_2H^+ + H_2 \rightarrow H_3^+ + N_2$	5.1×10^{-24}	66
2.38	$N_2H^+ + NH_3 \rightarrow NH_4^+ + N_2$	2.3×10^{-15}	66
2.39	$Ar^+ + NH_3 \rightarrow NH_3^+ + Ar$	1.6×10^{-15}	66
2.40	$ArH^+ + NH_3 \rightarrow NH_3^+ + H + Ar$	5.3×10^{-16}	66
2.41	$ArH^+ + NH_3 \rightarrow NH_4^+ + Ar$	1.6×10^{-15}	66
2.42	$ArH^+ + N_2 \rightarrow N_2H^+ + Ar$	8.0×10^{-16}	66
2.43	$N^+ + H \rightarrow H^+ + N$	2.0×10^{-16}	26
2.44	$H_2^+ + NH_3 \rightarrow NH_4^+ + H$	5.0×10^{-17}	26
2.45	$H_2^+ + NH_2 \rightarrow NH_3^+ + H$	5.0×10^{-17}	26
2.46	$H_2^+ + NH \rightarrow NH_2^+ + H$	5.0×10^{-17}	26
2.47	$NH^+ + NH_2 \rightarrow NH_2^+ + NH$	1.8×10^{-15}	26
2.48	$Ar^+ + NH_3 \rightarrow NH_2^+ + H + Ar$	5.5×10^{-17}	26
2.49	$Ar^+ + NH_3 \rightarrow ArH^+ + NH_2$	9.2×10^{-17}	26

The used K_k's for ion-molecule reactions are listed in Table III. Where possible, the rate coefficients are taken from a compilation by Anicich.[66] Anicich provides a collection of recommended values of rate coefficients for a wealth of bimolecular ion-molecule reactions for a gas temperature of 300 K. The gas temperature in the here investigated plasma is 460 K (see Sec. II C). However, this should not significantly influence the rate coefficients due to the fact that in most cases K is independent of T_g (see Ref. 23). Reaction coefficients which are not contained in Ref. 66 are taken from the following sources: Arakoni *et al.*[26] and Tao *et al.*[67]

TABLE IV. Considered ion wall loss reactions.

$H^+ + \mathrm{wall} \rightarrow H$	$NH^+ + \mathrm{wall} \rightarrow NH$	$N_2^+ + \mathrm{wall} \rightarrow N_2$
$H_2^+ + \mathrm{wall} \rightarrow H_2$	$NH_2^+ + \mathrm{wall} \rightarrow NH_2$	$N_2H^+ + \mathrm{wall} \rightarrow N_2 + H$
$H_3^+ + \mathrm{wall} \rightarrow H_2 + H$	$NH_3^+ + \mathrm{wall} \rightarrow NH_3$	$Ar^+ + \mathrm{wall} \rightarrow Ar$
$N^+ + \mathrm{wall} \rightarrow N$	$NH_4^+ + \mathrm{wall} \rightarrow NH_3 + H$	$ArH^+ + \mathrm{wall} \rightarrow Ar + H$

C. Wall loss for ions

We assume that ions reaching the wall recombine with a probability of 1. A compilation of the ion loss processes to the wall is shown in Table IV. For the case of dissociative recombination, the produced atomic hydrogen is assumed to be reflected from the surface with a probability of 1. The rate coefficients K_{wi} for the loss of positive ions to the walls are based on the uniform density discharge model for low and intermediate pressures of Lieberman and Lichtenberg[68]

$$K_{wi} = \frac{2h_{l,i}}{l_{el}}\sqrt{\frac{eT_e}{M_i}}. \tag{5}$$

M_i denotes the ion mass. The coefficient $h_{l,i}$ is given by[68,69]

$$h_{l,i} = \frac{0.86}{\sqrt{3 + \frac{l_{el}}{2\lambda_i}}}. \tag{6}$$

λ_i is the mean free path length for ions traversing the background gas j with density n_j

$$1/\lambda_i = \sum_{j,k} \sigma_k n_j. \tag{7}$$

σ_k denotes the cross section for the collision (reaction k) of the ion with the background gas atom or molecule j. These collisions can be elastic, but also charge exchange collisions and proton transfers can occur. The values for individual σ_k's are shown in Table V for a relative energy of $E_{ij} = 1.5 k_B T_g$ using

TABLE V. Total cross sections $\sum_k \sigma$ in 10^{-19} m^2 for collisions between ions i with background gas species j for a gas temperature of 460 K. Reference: a—σ taken from Bogaerts and Gijbels;[70] b—σ taken from Phelps;[71] c—σ determined from corresponding K (see Table III); d—assumed values (see text).

	$j = H_2$		N_2		Ar		NH_3	
$i = H^+$	9.8	(a)	8.6	(d)	8.6	(a)	16	(c)
H_2^+	7.1	(a)	8.8	(c)	8.5	(a)	24	(c)
H_3^+	8.5	(a)	9.8	(c)	9.5	(a)	23	(c)
N^+	2.1	(c)	12	(b)	12	(d)	21	(c)
NH^+	5.2	(c)	6.5	(c)	6.9	(d)	22	(c)
NH_2^+	0.8	(c)	10^{-4}	(d)	10^{-4}	(d)	21	(c)
NH_3^+	0.002	(c)	10^{-4}	(d)	10^{-4}	(d)	20	(c)
NH_4^+	10^{-5}	(d)	10^{-4}	(d)	10^{-4}	(d)	5.7	(c)
N_2^+	8.8	(c)	30	(b)	0.003	(c)	20	(c)
N_2H^+	10^{-8}	(c)	50	(c)	54	(d)	24	(c)
Ar^+	4.6	(a)	0.14	(c)	12	(a)	18	(c)
ArH^+	8.1	(a)	10	(c)	12	(a)	24	(c)

the gas temperature of $T_g = 460\,\mathrm{K}$ as obtained experimentally (see Sec. II C). Most cross sections and rate coefficients for the here considered reactions are available in the literature. However, some σ and K could not be found and, therefore, assumptions about the unavailable σ have to be made as these collisions cannot be neglected. For the collisions occurring in H_2-Ar plasmas, σ_k values are taken from Bogaerts and Gijbels[70] (label "a" in Table V). A detailed discussion of the reliability of these values was presented in Ref. 23. For collisions of N^+ and N_2^+ with N_2, $\sigma(E)$ values of Phelps[71] are used (label "b" in Table V). For those collisions where K is available in Table III (label "c" in Table V), σ is calculated from this corresponding K according to $K = \sigma(E_{ij}) \times (2E_{ij}/\mu_{ij})^{0.5}$ (μ_{ij}—reduced mass).[23] For the collisions of NH_x^+ ($x = 2, 3, 4$) with N_2 and NH_4^+ with H_2, we used an estimation of Anicich,[66] i.e., $\sigma = 1 \times 10^{-23}\mathrm{m}^2$, because they found that the corresponding K's are small for these reactions. For collisions of NH_x^+ ($x = 0;\ldots;4$) and N_2H^+ with Ar, no values for σ or K can be found (label "d" in Table V). In Refs. 72 and 73, it was discussed that the collision behavior between ions with N_2 and ions with Ar is similar which was also confirmed by the theoretically calculated rate coefficients in Ref. 74. Therefore, we used the missing σ or K for collisions of NH_x^+ ($x = 2, 3, 4$) and NH_4^+ with Ar from those values available for N_2. In Table V, this is indicated by "d." Similarly, for the collision of H^+ with N_2 σ is assumed to be the same as for H^+ with Ar. It should be noted that for the labels "a" and "b" in Table V elastic collisions are taken into account, whereas for the labels "c" and "d" elastic collisions are not taken into account because no corresponding σ or K data were reported in the literature. In this case, the value in Table V is a lower limit of the total cross section $\sum_k \sigma$. However, the influence of $\sum_k \sigma$ on K_{wi} is small as can be seen in Eq. (5): K_{wi} has an offset of $0.86/\sqrt{3}$ for the limit $\sum_k \sigma \to 0$ and varies only with the square root for higher $\sum_k \sigma$ (see Eq. (6)).

D. Further reaction sets

In this section, reactions involving excited species are presented and briefly explained. Metastables have a relatively long lifetime and can, therefore, collide quite often with the background gas j. As metastables carry potential energy of several eV, in a collision this energy can be transferred to j so that j can dissociate. To assess whether or not metastable argon Ar_{meta}, metastable molecular nitrogen $N_2(A)$, and the metastables N(D) and N(P) of atomic nitrogen influence the dissociation of molecules, they are considered in a simplified collisional-radiative model.[57,76] This model takes into account only the most important electronically excited states. The following species are considered

For the reaction set of excited Ar,

(1) Ar_{meta} consisting of the excited, metastable levels $1s^5$ and $1s^3$ in Paschen's notation.
(2) Ar_r consisting of the excited levels $1s^4$ and $1s^2$.
(3) Ar($2p$) consisting of the excited levels $2p^1$ to $2p^{10}$,

for the reaction set of excited N_2,

(1) N2(A) which denotes the excited, metastable level $N_2(A\,^3\Sigma_u^+)$.
(2) N2(B) which denotes the excited level $N_2(B\,^3\Pi_g)$.
(3) N2(C) which denotes the excited level $N_2(C\,^3\Pi_u)$.
(4) $N_2(a')$ which denotes the excited level $N_2(a'\,\Sigma_u)$,

and for the reaction set of excited N,

(1) N(D) which denotes the excited, metastable level N(^2D).
(2) N(P) which denotes the excited, metastable level N(^2P).

The considered reactions are summarized in Tables VI–VIII together with the corresponding rate coefficients. They are based on the reaction sets of Kimura and Kasugai.[57,76] Kimura and Kasugai take into account 16 reactions for the excited argon atom and 45 reactions for the excited molecular and atomic nitrogen (without mixed reactions of the type $Ar^* + N_2$). In a preparatory study (see Ref. 78), we found that these reaction sets can be reduced to 6 reactions for Ar, 23 reactions for N_2 and N, and 12 mixed reactions shown in Tables VI, VII, and VIII, respectively. These reactions are the dominant ones and they are sufficient to calculate the metastable densities $n_{X_{meta}}$ with X = Ar, N_2, and N with sufficient accuracy. For metastable Ar and N_2, the wall loss rate coefficient K_w is used[77,79]

$$\frac{1}{K_w} = \frac{\Lambda^2}{D} + \frac{V}{A}\frac{2(2-\beta)}{\beta}\frac{1}{v}, \tag{8}$$

($\Lambda = l_{el}/\pi$—diffusion length, D—diffusion constant,[54] $V/A = l_{el}/2$—volume-to-surface ratio for wall loss, β—surface loss probability of the considered species, value are listed in Tables VI and VII). Equation (8) was derived for neutrals diffusing through the plasma volume and are lost on the wall.[79] v is calculated by the mean velocity: $v = \sqrt{8k_BT/\pi M}$ with T and M being the temperature and mass of the considered species, respectively. For the wall loss rate coefficients of the metastables N(D) and N(P), Thorsteinsson and Gudmundsson[77] used the same values as for N in the ground state. Therefore, for N(D) and N(P) the same value as for N in the ground state is used here, too. The latter will be determined in Sec. IV (see Table VII).

IV. WALL LOSS TIMES OF RADICALS DETERMINED FROM AFTERGLOW MEASUREMENTS

For low-pressure plasmas, the main loss channel of radicals is the loss to the wall,[23,80–82] which can be expressed by a certain wall loss time t_{wrad}. The radical wall loss time t_{wrad} is usually described by a diffusive part and a surface loss part.[23,68] Hence, it is a function of the diffusion constant D_{rad}, the discharge geometry, the radical temperature T_{rad},

TABLE VI. Reaction set for excited argon with rate coefficients K for a reaction k (T_e in eV).

k	Reaction	$K(\mathrm{m^3s^{-1}})$	Reference
3.1	$e^- + Ar \to Ar_{meta} + e^-$	$5.0 \times 10^{-15} \times e^{-12.64/T_e}$	57
3.2	$e^- + Ar \to Ar(4p) + e^-$	$2.1 \times 10^{-14} \times e^{-13.13/T_e}$	57
3.3	$Ar_r \to Ar + h\nu$	1.0×10^5	57
3.4	$Ar(4p) \to Ar_r + h\nu$	3.0×10^7	57
3.5	$Ar(4p) \to Ar_{meta} + h\nu$	3.0×10^7	57
3.6	$Ar_{meta} + \mathrm{wall} \to Ar$	$K_{wAr_{meta}}$ ($\beta_{Ar_{meta}} = 1$)	75

TABLE VII. Reaction set for excited nitrogen with rate coefficients K for a reaction k (T_e in eV). t_{wN} denotes the wall loss time of N (see Sec. IV).

k	Reaction	$K(\mathrm{m^3 s^{-1}})$	Reference
4.1	$e^- + N_2 \rightarrow N_2(A) + e^-$	$1.2 \times 10^{-14} \times e^{-7.34/T_e}$	76
4.2	$e^- + N_2 \rightarrow N_2(B) + e^-$	$5.6 \times 10^{-15} \times e^{-6.81/T_e}$	76
4.3	$e^- + N_2 \rightarrow N_2(C) + e^-$	$6.4 \times 10^{-15} \times e^{-9.87/T_e}$	76
4.4	$e^- + N_2 \rightarrow N_2(a) + e^-$	$5.1 \times 10^{-15} \times e^{-11.69/T_e}$	76
4.5	$e^- + N_2(A) \rightarrow N_2^+ + 2e^-$	$8.3 \times 10^{-15} \times e^{-12.84/T_e}$	76
4.6	$e^- + N_2(B) \rightarrow N_2^+ + 2e^-$	$2.1 \times 10^{-14} \times e^{-11.0/T_e}$	76
4.7	$e^- + N_2(a) \rightarrow N_2^+ + 2e^-$	$4.3 \times 10^{-14} \times e^{-10.32/T_e}$	76
4.8	$e^- + N \rightarrow N(D) + e^-$	$2.7 \times 10^{-14} T_e^{-0.4} \times e^{-3.35/T_e}$	76
4.9	$e^- + N \rightarrow N(P) + e^-$	$9.1 \times 10^{-14} T_e^{-0.45} \times e^{-4.80/T_e}$	76
4.10	$e^- + N(D) \rightarrow N^+ + 2e^-$	$1.0 \times 10^{-14} T_e^{-0.36} \times e^{-0.83/T_e}$	76
4.11	$e^- + N(P) \rightarrow N^+ + 2e^-$	$5.5 \times 10^{-15} T_e^{-0.41} \times e^{-1.05/T_e}$	76
4.12	$N_2(a) + N_2(A) \rightarrow N_2^+ + e^-$	9.0×10^{-18}	76
4.13	$2N_2(a) \rightarrow N_2^+ + e^-$	2.5×10^{-17}	76
4.14	$N_2(A) + N \rightarrow N(P) + N_2$	5.0×10^{-16}	76
4.15	$N_2(A) + N_2 \rightarrow 2N_2$	4.0×10^{-17}	76
4.16	$N(P) + N(D) \rightarrow N_2^+ + e^-$	3.0×10^{-18}	76
4.17	$N_2(B) \rightarrow N_2(A) + h\nu$	2.0×10^5	76
4.18	$N_2(C) \rightarrow N_2(B) + h\nu$	2.7×10^7	76
4.19	$N_2(A) + \text{wall} \rightarrow N_2$	$K_{wN_2(A)}$ $(\beta_{N_2(A)} = 1)$	77
4.20	$N_2(a) + \text{wall} \rightarrow N_2$	$K_{wN_2(a)}$ $(\beta_{N_2(a)} = 1)$	76
4.21	$N(D) + \text{wall} \rightarrow 0.5N_2$	$K_{wN(D)} = (t_{wN})^{-1}$	
4.22	$N(P) + \text{wall} \rightarrow 0.5N_2$	$K_{wN(P)} = (t_{wN})^{-1}$	

and the surface loss probability β_{rad} (see Eq. (8)). In our experiment, the geometry of the plasma chamber does not exhibit a simple cylindrical geometry and the plasma-surrounding walls consist of different materials which have different β_{rad}. Furthermore, the radical temperature is *a priori* not known since radicals are mainly produced by dissociation, which is accompanied by a release of potential Franck-Condon energy[44] and T_{rad} can, therefore, exceed the gas temperature considerably. β_{rad} is a function of the radical species,[49,83] the surface material,[50,81,83,84] but most likely also a function of the surface condition[85] (for example, substrate temperature and roughness) and even the plasma parameters[81,86] (for example, ion flux). Values of β_{rad} for one radical species and the same surface material can vary up to an order of magnitude in the literature (compare values in Refs. 50, 80, 81, and 86 or in Refs. 49 and 87). Furthermore,

TABLE VIII. Reaction set with rate coefficients K for reactions k involving excited species.

k	Reaction	$K(\mathrm{m^3 s^{-1}})$	Reference
5.1	$Ar_{meta} + H_2 \rightarrow 2H + Ar$	1.1×10^{-16}	57
5.2	$Ar_r + H_2 \rightarrow 2H + Ar$	1.1×10^{-16}	57
5.3	$Ar_{meta} + N_2 \rightarrow N_2(C) + Ar$	3.0×10^{-17}	76
5.4	$N_2(A) + H \rightarrow N_2 + H$	5.0×10^{-17}	39
5.5	$N_2(A) + H_2 \rightarrow N_2 + 2H$	2.0×10^{-16}	39
5.6	$N_2(A) + NH_3 \rightarrow N_2 + NH_3$	1.6×10^{-16}	39
5.7	$N_2(B) + H_2 \rightarrow N_2(A) + H_2$	2.5×10^{-17}	39
5.8	$N_2(a) + H \rightarrow N_2 + H$	1.5×10^{-17}	39
5.9	$N_2(a) + H_2 \rightarrow N_2 + 2H$	2.6×10^{-17}	39
5.10	$N(D) + H_2 \rightarrow NH + H$	2.3×10^{-18}	39
5.11	$N(D) + NH_3 \rightarrow NH_2 + NH$	1.1×10^{-16}	39
5.12	$N(P) + H_2 \rightarrow NH + H$	2.5×10^{-20}	39

it has to be kept in mind that β_N values are in general determined from measured data on the basis of a diffusion model, which describes the transport of the radical particles to the chamber walls. This evaluation procedure depends to a large extent on assumptions on the relevant geometry of the plasma chamber and on the assumption about the radical temperature. Summarizing, describing t_{wrad} by a model is not possible due to unknown input parameters. In the present work, another approach is realized: t_{wrad} is measured directly for selected plasma conditions. This is done by monitoring the radical density in the temporal afterglow of the plasma. In this phase, the production process of radicals (electron-induced dissociation) is terminated within microseconds[88] and the only important loss process is the loss to the wall.[50,80,81,86] The relative radical densities for the radical species H, N, NH, and NH_2 are measured by ionization threshold mass spectrometry in a pulsed plasma (see Sec. II F).

The aim is to determine the wall loss time t_{wrad} of the radical particles in the H_2-N_2-Ar plasma at 1.5 Pa. However, at 1.5 Pa H_2-N_2-Ar plasmas do not ignite reliably so that an operation in a pulsed mode for measuring the decay time is not possible. Only at higher pressures equal to or greater than 3.0 Pa, H_2-N_2-Ar plasmas ignite reliably for all studied N_2 partial pressure fraction. However, when using deuterium instead of protium, i.e., D_2-N_2-Ar, ignites reliably even at 1.5 Pa plasma. Therefore, a D_2-N_2-Ar plasma is studied. The transferability of the results of D_2-N_2-Ar to the H_2-N_2-Ar plasma is investigated at 3.0 Pa for nearly identical plasma conditions. In addition, measurements in a pure H_2 and D_2 plasma are performed. For the mixed D_2-N_2-Ar plasma, t_{wrad} was measured for only two N_2 partial pressure fractions at 1.5 Pa in the pulsed plasma mode as the ITMS measurements are elaborate and time consuming.

Wall loss times t_{wrad} are determined from the temporal decay curves in the afterglow of the plasma. For the plasma conditions $p = 1.5$ Pa, $f_{N_2} = 21\%$, *rf* power 200 W, $t_{on} = 3$ ms, and $t_{off} = 10$ ms, the measured signals of the relative densities of D, N, and ND in the pulsed plasma are shown in Fig. 1 as a function of time t. The time axis is chosen such

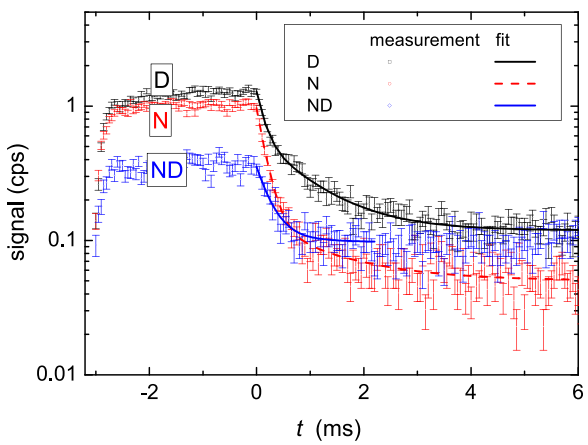

FIG. 1. Plasma monitor signal on mass channels 2, 14, and 16 amu/e at electron energies of 15, 18, and 16 eV, respectively, in a pulsed D_2-N_2-Ar plasma for the plasma conditions $p = 1.5$ Pa, $f_{N_2} = 21\%$, $P_{rf} = 200$ W, $t_{on} = 3$ ms, and $t_{off} = 10$ ms.

that at $t = 0$ the power-off phase begins. The power-on (P_{on}) phase ($t_{on} = 3$ ms) is characterized by a signal increase within the first 0.3 ms of the pulse followed by a region between −2 and 0 ms, where the signal is maximal and constant. The P_{off} phase is characterized by a strong decrease of the signal. The signal drop in the first 1 ms is substantially faster than for $t \gtrsim 1$ ms. For large t in the P_{off} phase, the signal exhibits a small background. The signal in the P_{off} phase can be well described by a function, which is the sum of two exponentials and a constant background:

$$y = C_1 e^{-t/t_{wrad}} + C_2 e^{-t/t_{wrad,2}} + y_0. \quad (9)$$

C_1, C_2, and y_0 are fitting constants, $t_{wrad,2}$ is the time constant of the slowly decaying part. The fit curve is included in Fig. 1. For all studied mixed plasmas, Eq. (9) is used for fitting the measured decay curves. The wall loss times obtained in this way for all studied plasma conditions can be found in Table IX. The wall loss times are in the range between 0.1 and 0.6 ms. If the pressure is decreased from 3.0 to 1.5 Pa, the wall loss times t_{wD} and t_{wN} also decrease by a factor of 2 for all studied f_{N_2}. At a constant pressure of 1.5 Pa but decreasing nitrogen partial pressure fraction from $f_{N_2} = 21\%$ to $f_{N_2} = 3.3\%$, t_{wN} decreases by a factor of 1.6. For ND, t_{wND} decreases moderately with decreasing p, independently from the studied f_{N2}.

For ND_2, the wall loss time t_{wND_2} could not be measured. For a mass spectrometer cathode voltage of 14 eV, both ND_2 and H_2O produce ions leading to a signal on mass channel 18 amu/e. It is observed that the signal on this mass channel does not vary in a pulsed plasma in the investigated time range of 10 ms. Therefore, most likely the measured signal on mass channel 18 amu/e originates dominantly from H_2O from the residual gas of the PM chamber.

The wall loss times of H and D in the H_2-N_2-Ar and D_2-N_2-Ar plasma at 3.0 Pa differ only slightly. We assume that the wall loss time is the same for protonated and deuterated species, i.e., shows no isotope effect. Therefore, the wall loss times measured for the deuterated case will in the following also be applied for the H_2-N_2-Ar plasma.

The wall loss times of the radicals H, N, NH, and NH_2 used in the model are the mean values of the two measurements for a pressure of 1.5 Pa, i.e., mean values of the two last lines in Table IX for each species. In detail, these are $t_{wH} = 0.16$ ms for H, $t_{wN} = 0.23$ ms for N, and $t_{wNH} = 0.29$ ms for atomic hydrogen. Since for NH_2 no experimental data could be obtained, the value of NH, i.e., $t_{wNH_2} = 0.29$ ms is used assuming they behave similarly. It is assumed that these wall loss times are valid as model input parameters of the studied H_2-N_2-Ar plasma for a total pressure of 1.5 Pa (see Sec. V) for the studied N_2 partial pressure fractions of 3.3% and 21% (as measured, see Table IX) and are used as approximation for all other considered N_2 partial pressure fractions. We want to note here that calculating t_{wrad} with β_{rad} values taken from the literature[7] would lead to significantly different results of the rate equation model and, hence, different radical densities which differ up to two orders of magnitude from the values for our case. For a detailed discussion of the discrepancy of β_{rad} between our and other groups, see Refs. 43 and 44.

TABLE IX. Measurement results of the wall loss time t_{wrad} of radicals from plasma monitor afterglow measurements for various pressures p and partial pressure fractions f_j. H_2-N_2-Ar and D_2-N_2-Ar plasmas are studied at 3.0 Pa (power 300 W, $t_{on} = 10$ ms, $t_{off} = 20$ ms) and 1.5 Pa (power 200 W, $t_{on} = 3$ ms, $t_{off} = 10$ ms).

p (Pa)	f_{H_2} (%)	f_{D_2} (%)	f_{N_2} (%)	f_{Ar} (%)	f_{NH_3} (%)	$t_{wH/D}$ (ms)	t_{wN}	$t_{wNH/ND}$	t_{wNH_2}
3.0	69	0	21	1.5	8.5	0.33	0.30	0.64	0.40
3.0	0	67[a]	21[a]	1.8[a]	10.2[a]	0.28	0.34	0.39	
1.5	0	67	21	1.8	10.2	0.14	0.17	0.27	
1.5	0	92	3.3	1.5	3.2	0.17	0.28	0.31	

[a]Extrapolated values from 1.5 Pa measurements since same gas flows were used.

V. RESULTS

A. Partial pressures

The partial pressure fractions f_j determined with the MBMS before and during plasma operation are shown in Fig. 2. As can be seen in Fig. 2, the gas composition during the plasma-on phase differs slightly from that during the plasma-off phase. In particular, f_{N_2} decreases during plasma operation. The gas composition is plotted against $f_{N_2} = f_{N_2}(P_{on})$ because the rate equation model calculates with f_j of the P_{on} phase. The N_2 partial pressure fraction is varied and the investigated values of f_{N_2} are 0.02%, 0.8%, 1.6%, 3.4%, 7.9%, 20%, 36%, and 56%. The lowest f_{N_2} for zero input of N_2 is 0.02 since a tiny amount of nitrogen is also present in the pure H_2-Ar plasma. This small nitrogen partial pressure fraction is probably due to N_2 release from the chamber walls during plasma operation. For simplicity, this will in the following be called $f_{N_2} = 0\%$.

Despite constant gas supply, f_{Ar} (P_{off}) increases slightly from 1.2% ($f_{N_2} = 0\%$) to 1.5% ($f_{N_2} = 56\%$), which is attributed to the change in the pumping speed by changing the gas mixture (from $j = H_2$ with mass $M = 2$ amu to N_2 with 28 amu). If a gas with particles of high mass is mixed with a gas

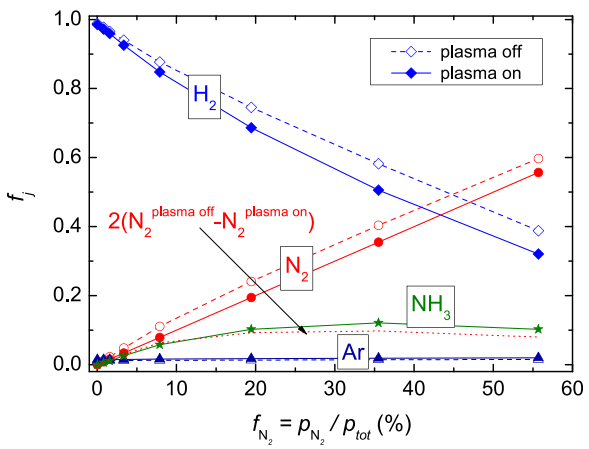

FIG. 2. Partial pressure fractions f_j of $j = H_2$, N_2, Ar, and NH_3 measured with the molecular-beam mass spectrometer as a function of $f_{N_2} = f_{N_2}(P_{on})$ for a total pressure of 1.5 Pa and an *rf* power of 200 W during plasma-off (open symbols) and plasma-on phase (solid symbols).

with low mass, the light and fast particles accelerate the heavy particles, so that the gas of heavy particles is pumped faster.[89] At plasma ignition, the total pressure of $p = 1.5$ Pa decreases at most by 4% for N_2 partial pressure fractions of $f_{N_2} > 5\%$. For lower N_2 partial pressure fractions p remains constant within the measurement accuracy of $\pm 2\%$ during plasma ignition.

B. Ammonia

In addition to the three stable gas species H_2, N_2, and Ar originating from the input gas flow, the fourth species ammonia (NH_3) appears during plasma operation. Ammonia has a higher partial pressure fraction than Ar, but a lower partial pressure fraction than N_2. At $f_{N_2} = 36\%$, f_{NH_3} has a maximum with a partial pressure fraction of 12.1%. The f_{H_2} ratio between P_{on} and P_{off} decreases with increasing f_{N_2} from $f_{H_2}(P_{on})/f_{H_2}(P_{off}) = 1$ to 0.83. The f_{N_2} ratio between P_{on} and P_{off} is between $f_{N_2}(P_{on})/f_{N_2}(P_{off}) = 0.68$ and 0.93. With respect to the nitrogen balance, we can state the following: the nitrogen atoms which appear as NH_3 are compared with the missing nitrogen atoms of the N_2 gas input. The latter corresponds to twice the difference of the N_2 density between the plasma-off and plasma-on phase. This missing nitrogen partial pressure fraction of $2 \times (f_{N_2}(P_{off}) - f_{N_2}(P_{on}))$ is shown in Fig. 2 and matches f_{NH_3} very well. This agreement shows that the missing N_2 during P_{on} appears as NH_3.

In the following, the production of ammonia is shortly discussed. One pathway that could lead to ammonia production is gas phase reactions. Calculating the NH_3 density with the rate equation model (see Sec. III) taking into account only volume reactions producing NH_3 shows that the calculated NH_3 density is in the whole f_{N_2} range 4 orders of magnitude below the measured NH_3 density of Fig. 2. That means that volume reactions producing NH_3 play only a negligible role. Therefore, NH_3 must be produced on the plasma surrounding walls. It is generally accepted that one mechanism for ammonia production is based on the adsorption of atomic hydrogen and nitrogen on surrounding surfaces followed by gradual recombination of adsorbed atomic nitrogen N(s) and hydrogen H(s) to NH_3 with NH(s) and NH_2(s) as intermediate reaction products. For a detailed model, see Refs. 3, 30, and 38. A quantitative description of NH_3 production is not attempted in the present work since this surface reaction model would require the input of several unknown parameters. For example, in the H_2-N_2 mixture it is unclear to what extent H returns as H_2 and as NH_3 from the wall, i.e., the partial surface recombination probabilities of H recombining with adsorbed species at the wall are not known. In the following, the measured NH_3 density is taken as an input parameter in the model because the used model does not account for surface reactions for the production of NH_3.

With respect to the f_{NH_3}, we would like to add the following note summarizing some additional experimental results: The maximum of f_{NH_3} at $f_{N_2} = 36\%$ and the f_{NH_3} dependence as a function of f_{N_2} are also observed for an H_2-N_2-Ar plasma with 3.0 Pa and for a D_2-N_2-Ar plasma with 1.5 Pa for otherwise identical plasma conditions. The production of NH_3, therefore, seems to be not significantly influenced by a pressure increase by a factor of 2 or an exchange of H_2 with D_2. For a power variation from 100 to 600 W ($p = 1.5$ Pa, H_2-N_2-Ar, $f_{N_2} = 3.4\%$, $f_{Ar} = 1.5\%$), a nonmonotonic increase of f_{NH_3} is observed. In this power variation, T_e stays approximately constant, n_e increases linearly from 2.8×10^{15} m^{-3} to 3.2×10^{16} m^{-3} and the measured hydrogen dissociation degree n_H/n_{H_2} also increases linearly from 0.0023 to 0.024 with increasing power. In an earlier publication, it was shown that n_H/n_{H_2} is proportional to n_e (Ref. 23) (see also Sec. V D) and this trend is here confirmed. Furthermore, from the model we find that also the atomic nitrogen density increases linearly with increasing n_e and, hence, increasing power. However, the measured f_{NH_3} increases nonmonotonically. From 100 to 300 W, f_{NH_3} increases from 1.7% to 3.1%. From 300 to 600 W, f_{NH_3} increases from 3.1% to 3.9%. In summary, the relatively high ammonia fraction of several percent was proven for a broad variation of plasma conditions.

Chen *et al.*[32] examined an inductively coupled plasma at 1 Pa and 400 W rf power. They measured the NH_3 density with a quadrupole mass spectrometer for plasma conditions comparable with the present study. They studied n_{NH_3} in a remote area (chamber material: stainless steel) connected with the plasma chamber by a 5 mm orifice. A f_{N_2} variation showed that the NH_3 density exhibited a maximum of $n_{NH_3} = 2 \times 10^{19}$ m^{-3} for $f_{N_2} = 40\%$. This n_{NH_3} corresponds to a NH_3 partial pressure fraction of 8% of the total gas density for which a gas temperature $T_g = 300$ K is assumed. Since NH_3 is produced on the chamber wall, consequently, the NH_3 production depends on the surface area of the chamber wall, which is different between Chen *et al.* and the present study. Despite the differences in the design of the plasma chamber resulting in different surface areas between the experiments by Chen *et al.* and the present work, both the maximum of the NH_3 partial pressure fraction as well as the position of the maximum agree surprisingly well with each other (present work: maximum of $f_{NH_3} = 12\%$ for $f_{N_2} = 36\%$).

C. Electron temperature and density

T_e is on the one hand experimentally measured with the Langmuir probe and on the other hand determined with the rate equation model. As described in Sec. III in our model, T_e is fitted to fulfill the quasi-neutrality condition. The measured and fitted electron temperatures are plotted in Fig. 3 as a function of f_{N_2}. The measured T_e of the hydrogen plasma with 1.2%-Ar partial pressure fraction ($f_{N_2} = 0\%$) is 4.4 eV. With increasing N_2, the measured T_e decreases monotonically reaching 3.2 eV for $f_{N_2} = 56\%$. The modeled T_e shows the same behavior as the measured T_e. The calculated values agree with the measured ones within the experimental uncertainty but are systematically at slightly (about 0.2 eV) higher values. All in all, the rate equation model describes T_e very well. In Fig. 3, also the electron density n_e is shown which was obtained experimentally by Langmuir probe measurement. n_e increases with increasing f_{N_2} monotonically from 0.8×10^{16} m^{-3} at $f_{N_2} = 0\%$ to 2×10^{16} m^{-3} at $f_{N_2} = 56\%$.

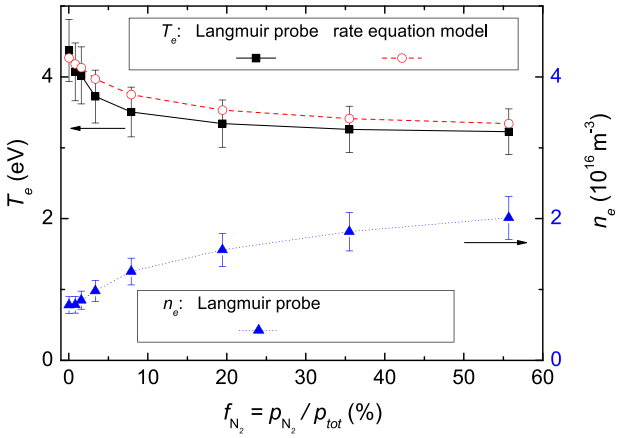

FIG. 3. Measured and modeled electron temperature T_e as well as measured electron density n_e.

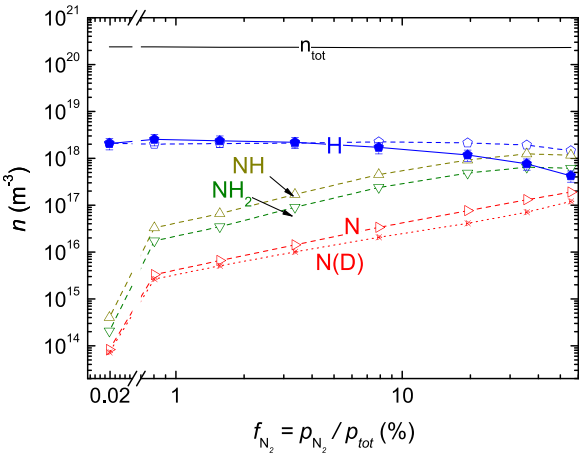

FIG. 4. The calculated densities (open symbols) of the radicals H, N (ground state N and metastable state N(D)), NH, and NH_2 as a function of f_{N_2} (first value at $f_{N_2} = 0.02\%$). In addition, the H density measured by optical emission spectroscopy and actinometry is shown (solid symbols). For comparison, the total density n_{tot} of the gas mixture is plotted.

D. Radical densities

The absolute densities of the radical particles are calculated with the rate equation model described in Sec. III. The key input parameters for the rate equation model for calculating n_{rad} are f_j (power-on phase; including NH_3), n_e, and t_{wrad}. The results for the calculated radical densities are shown in Fig. 4. The calculated density of atomic hydrogen n_H is in the range of $0.0 \leq f_{N_2} \leq 10\%$ roughly constant at 2×10^{18} m^{-3} and decreases slightly with further increasing f_{N_2}. The densities of atomic nitrogen in the ground state and in the metastable state N(D) as well as n_{NH} and n_{NH_2} increase monotonically. At $f_{N_2} = 0.8\%$, n_H is more than two orders of magnitude higher than the other densities considered here. At $f_{N_2} > 15\%$, n_H, n_{NH}, and n_{NH_2} show comparable densities, while those of n_N and n_N (D) are still substantially lower.

In addition to the modeled values, the measured hydrogen density determined by OES and actinometry is shown in Fig. 4 (see Sec. II C). Densities of nitrogen and ammonia could not be measured with OES since no suitable emission lines were observed. For low N_2 partial pressure fraction ($f_{N_2} < 7.9\%$), the measured n_H agrees with the calculated values within the experimental uncertainty. With increasing f_{N_2} ($f_{N_2} > 7.9\%$), the measured n_H decreases considerably, whereas the calculated density decreases slightly resulting in a significant deviation between model and experiment. The deviation in n_H between model and experiment is attributed to the dependence of the H wall loss time, i.e., the surface loss probability β_H on f_{N_2} (for details, see Ref. 54), which is not taken into account in the model. With increasing N_2 partial pressure fraction, β_H increases and thus n_H decreases. The increase of β_H with increasing f_{N_2} is attributed to the recombination of H to NH_3 on the surface, which occurs in H_2-N_2 mixed plasmas in addition to the recombination of H to H_2 (see also Ref. 54).

In Table X, the most important reactions for the production of the radicals with their corresponding relative reaction rates R_k/R_{tot} are summarized. A reaction rate R_k is the product of the educt densities and the rate coefficient K_k of a reaction k (for the considered reactions, see Sec. III). The sum of the production reactions of a species is $R_{tot} = \sum_k R_k$. In all shown cases, the most important reaction for the production of the radical particles is the electron-collision-induced dissociation of the parent molecules. In the examined H_2-N_2-Ar plasma, the electron-collision-induced dissociation contributes more than 50% to the total production rate R_{tot}. Other reactions with fractions in the range of 10%–20% of R_{tot} can be found in Table X. The only significant loss process for the radical particles is the wall loss. The relative loss rate R_{wrad}/R_{tot} is greater than 88% for all considered radicals. Losses through other channels play only a minor role at that pressure of 1.5 Pa. For example, for the loss of ground-state N, reactions 4.9 (electron collision) and 4.14 (collisions with N_2 metastables) contribute to R_{tot} and contribute together at most 10% to the loss of ground-state N.

TABLE X. Most important reactions k for the production of the radical species H, N, NH, and NH_2. In addition, the relative reaction rates R_k/R_{tot} are presented for $f_{N_2} = 0.8\%$ and $f_{N_2} = 56\%$. Only reactions with $R_k/R_{tot} > 10\%$ are shown.

Species	Reaction	k	R_k/R_{tot} ($f_{N_2} = 0.8\%$) (%)	R_k/R_{tot} ($f_{N_2} = 56\%$) (%)
H	$e^- + H_2 \rightarrow 2H + e^-$	1.1	89	56
	$e^- + NH_3 \rightarrow NH_2 + H + e^-$	1.19	<10	18
N	$e^- + N_2 \rightarrow N + N(D) + e^-$	1.6	88	89
NH	$e^- + NH_3 \rightarrow NH + H_2 + e^-$	1.21	83	84
	$e^- + NH_3 \rightarrow NH + 2H + e^-$	1.20	15	<10
NH_2	$e^- + NH_3 \rightarrow NH_2 + H + e^-$	1.19	91	79

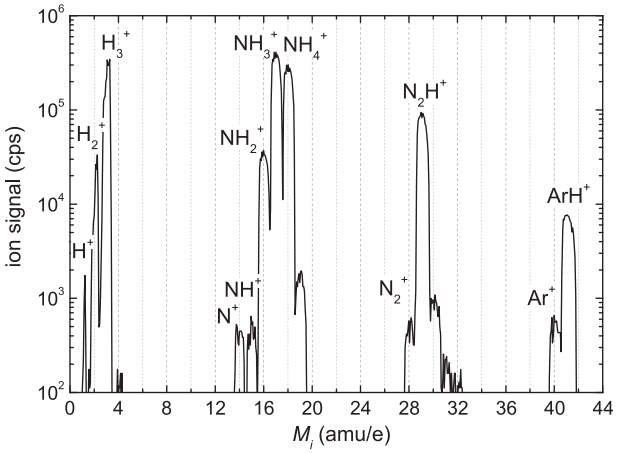

FIG. 5. Ion mass spectrum for $f_{N_2} = 3.4\%$.

We would like to note that the reaction set for the excited species was included in the model to study whether there is an influence of the metastable species on the production of radicals or not. To conclude, N(D) has a noticeable influence and the N(D) density is of the order of the ground state N density. However, other metastables as $N_2(A)$ and N(P) have only a negligible influence on the dissociation in the studied plasma. The influence of Ar_m is also negligible due to low Ar content.

E. Ion mass spectrum

Before the experimentally obtained ion densities are presented, first one example of a raw signal is shown in Fig. 5. The ion raw signals cannot be quantitatively compared with each other because they are not calibrated. But, the calibration does not change the signals by orders of magnitude such that rough trends can already be discussed based on the presented ion mass spectrum. In Fig. 5, the PM raw signal for the ion mass spectrum is shown for a N_2 partial pressure fraction of 3.4%. The discriminator voltage V_{PM} in the plasma monitor is set to the maximum of the ion energy distributions (IED) at 21 V. The maxima of the IEDs of H^+, H_2^+, and H_3^+ are 2 V lower at 19 V than for the other considered ionic species. Therefore, the real maxima for these H_x^+ ions are by a factor of about 3 higher than they appear in Fig. 5 (for details, see Sec. II E). The highest signals in Fig. 5 originate from the ions H_3^+ (at 3 amu/e), NH_3^+ (17 amu/e), NH_4^+ (18 amu/e), and N_2H^+ (29 amu/e). One order of magnitude lower are the signals of the H_2^+ (2 amu/e), NH_2^+ (16 amu/e), and ArH^+ (41 amu/e). An additional magnitude lower are the signals of H^+ (1 amu/e), N^+ (14 amu/e), NH^+ (15 amu/e), N_2^+ (28 amu/e), and Ar^+ (40 amu/e). All these ionic species will be discussed in this work. The ion densities will be determined from the signals of the ion mass spectra according to the procedure described in Sec. II E. Signals on other mass channels are not considered in this work. It should be mentioned that the signals of Fig. 5 occurring at $M_i = 19$ amu/e and $M_i = 30$ amu/e are attributed to $^{15}NH_4^+$ and $N_2H_2^+$, respectively. For details, see Ref. 54.

F. Ion densities of the most abundant ions

The ions with the highest ion densities in the studied H_2-N_2-Ar plasma are shown in Fig. 6. H_3^+ is the dominant ion in the range of $0.0 \le f_{N_2} < 3.4\%$. In this range, the H_3^+ density decreases with increasing f_{N_2}. For $3.4 < f_{N_2} < 40\%$, NH_3^+ and NH_4^+ show the highest densities and agree with each other within the experimental uncertainty. Finally, N_2H^+ is the dominant ion at $f_{N_2} = 56\%$, but NH_3^+ and NH_4^+ have only a slightly lower density. The most striking observation in Fig. 6 is the fact that even at rather low f_{N_2} (>3.4%) the dominant ions are NH_3^+ and NH_4^+. This dominance is at first glance unexpected as these ions do not originate from the dominant background gas species H_2, but from NH_3. For $f_{N_2} = 3.4\%$, NH_3 has a partial pressure fraction of $f_{NH_3} = 2.6\%$ and it does not exceed 12% for all considered f_{N_2}. Although f_{N_2} is quite low compared with the H_2 partial pressure fraction, NH_3^+ and NH_4^+ are the dominant ion species. The electron density n_e determined by the Langmuir probe is also shown in Fig. 6. It has to be kept in mind, the total ion density is set equal to the electron density due to the quasi-neutrality (see Sec. II E).

G. Ion densities—Comparison between experiment and model

The measured and modeled ion densities are compared in Figs. 7 and 8 as a function of f_{N_2}. The ion species containing nitrogen are shown in Fig. 8, while all others are shown in Fig. 7. The densities of the dominant ion species H_3^+ (Fig. 7), NH_3^+, NH_4^+, and N_2H^+ (Fig. 8), which have densities of more than 1×10^{15} m^{-3}, have already been described in Sec. V F (Fig. 6). Please note that the data in Fig. 6 are shown on a linear scale, while data in Figs. 7 and 8 are plotted on double logarithmic scale. The experimental data show the following behaviors: The densities of H_2^+, ArH^+, and NH_2^+ are predominantly in the range of 10^{14} m^{-3}. While H_2^+ and ArH^+ (Fig. 7) decrease slightly with increasing f_{N_2}, NH_2^+ (Fig. 8) increases by one order of magnitude in the range of $0.8 \le f_{N_2} \le 56\%$. The density of N_2^+ is for $f_{N_2} = 0.8\%$ more than 3 orders of magnitude below n_e, but increases with increasing f_{N_2} by about a factor of 300. Ion species with

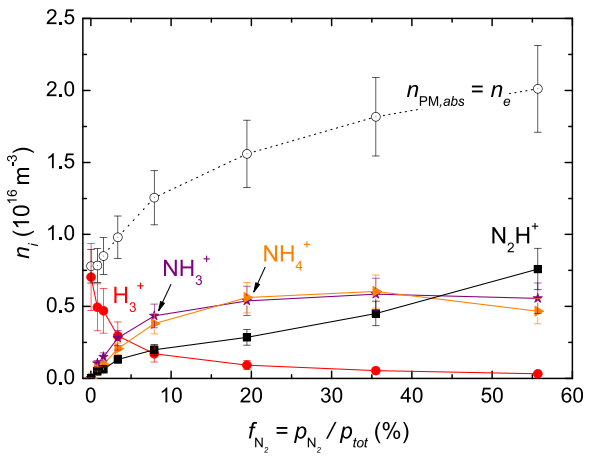

FIG. 6. Measured densities n_i of the most abundant ions. The total ion density $n_{PM,abs}$ corresponds to the electron density n_e.

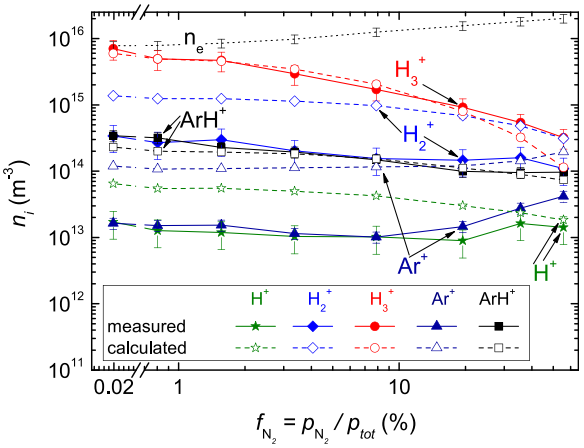

FIG. 7. Measured and calculated ion densities n_i of H_x^+ ($x = 1 - 3$), Ar^+, and ArH^+ as well as n_e.

densities less than 1×10^{14} m^{-3} are H^+, Ar^+, N^+, and NH^+. n_{H^+} and n_{Ar^+} (Fig. 7) vary only slightly with varying f_{N_2}. n_{N^+} and n_{NH^+} (Fig. 8) increase with f_{N_2} in the range of $0.8 \leq f_{N_2} \leq 56\%$ by almost two orders of magnitude, but remain only minor contributions to the total ion density. As discussed in Sec. V A, a tiny amount of nitrogen ($f_{N_2} = 0.02\%$) is also present in the pure H_2-Ar plasma (probably released from the wall during plasma operation) and accordingly $N_xH_y^+$ ions are observed but their densities remain below 3×10^{13} m^{-3}.

In general, the modeled densities are in satisfactory agreement with the experimental data. In the following, the similarities and differences between the model results and the experimental data are briefly discussed. We classify the model data into 3 groups: agreement within 20%, within a factor of 2, and within a factor of 10.

The calculated ion densities of $n_{H_3^+}$ in the range of $f_{N_2} \leq 20\%$ and n_{ArH^+} in range of $1.6 \leq f_{N_2} \leq 36\%$ fit the experimental densities within a maximum deviation of 20%, which means they fit within the experimental accuracy of the measured ion densities. The calculated ion densities of N^+, NH^+, NH_2^+, NH_4^+, and N_2H^+ agree in the complete range of studied f_{N_2} with the experimental densities within a factor of 2.

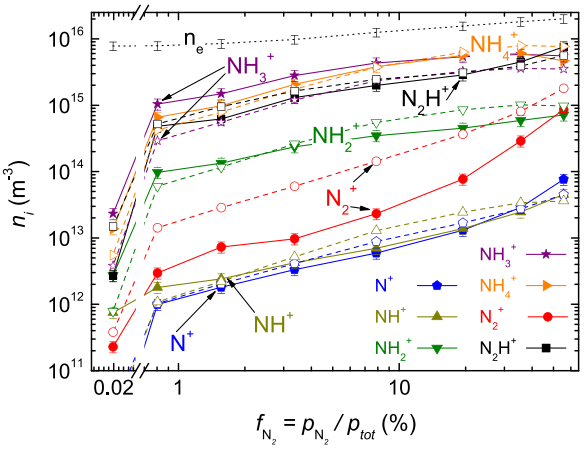

FIG. 8. Measured (solid symbols) and calculated (open symbols) ion densities n_i of NH_x^+ ($x = 0 - 4$), N_2^+, and N_2H^+ as well as n_e.

The same holds for NH_3^+ for $f_{N_2} > 5\%$. The calculated densities n_{N^+}, n_{NH^+}, $n_{NH_2^+}$, and $n_{N_2H^+}$ intersect the measured ones. Calculated ion densities which differ from the experimental densities between a factor of 2 and 10 are the densities of H^+, H_2^+, N_2^+, and Ar^+. They all show a similar dependence on f_{N_2} as the measured densities but are all significantly higher. We note that H_2^+, N_2^+, and Ar^+ are the primary ion species which are produced by direct electron-induced ionization of the background gas species H_2, N_2, and Ar, respectively. However, H^+ is also a primary ion, but has in contrast to the before-mentioned ion species further important production channels, i.e., electron-induced dissociative ionization from various mother molecules. A possible reason for this deviation will be discussed in the following.

We emphasize again that the applied rate equation model for the H_2-N_2-Ar plasma is, on the one hand, zero-dimensional and, therefore, simplified, but on the other hand, very complex with respect to the plasma-chemical reactions. The rate equation model considers 30 different species and more than 150 reactions. Some species densities are strongly dependent on other species densities. Despite this substantial complexity, most of the calculated ion densities match the measured values within a factor of 2. This agreement is remarkable and probably all that can be anticipated from such a model. The main features, i.e., the dominant ion species for different N_2 partial pressure fractions and the dependence of the ion densities and the electron temperature on f_{N_2}, are reproduced by the model.

In spite of the acceptable general agreement, some quantitative deviations between model and experiment remain. The main quantitative difference is that the densities of the primary ions H_2^+, N_2^+ and Ar^+ are clearly overestimated by the model. A sensitivity analysis—similarly as in a former publication[23] where the model input parameters were varied—showed that the plasma cylinder height l_{el} is a key parameter. A slight improvement in the description of these primary ions can be achieved when l_{el} was increased. In doing so, the calculated densities of the primary ions decrease with increasing l_{el} since the rate of ion-molecule collisions in the plasma volume increases. However, to achieve a satisfactory agreement l_{el} has to be increased by a factor of 3, which is physically not very reasonable. Simulations of the ion densities in less complex plasmas, i.e., H_2-Ar and H_2-He, have shown that the used l_{el} of 0.06 m is reasonable for the considered pressure range and describes the measured ion densities well. To investigate this discrepancy between model and experiment for the primary ion densities more accurately, studies with a spatially resolved modeling in the form of a particle-in-cell simulation might give insights, which are not accessible with the present zero-dimensional model.

VI. DISCUSSION

A. Ion chemistry

Based on the rate equation model, the ion chemistry will be explained in the following. For that purpose, the most important reactions for production and loss of the most common ion species are sketched in Fig. 9 for three different f_{N_2}.

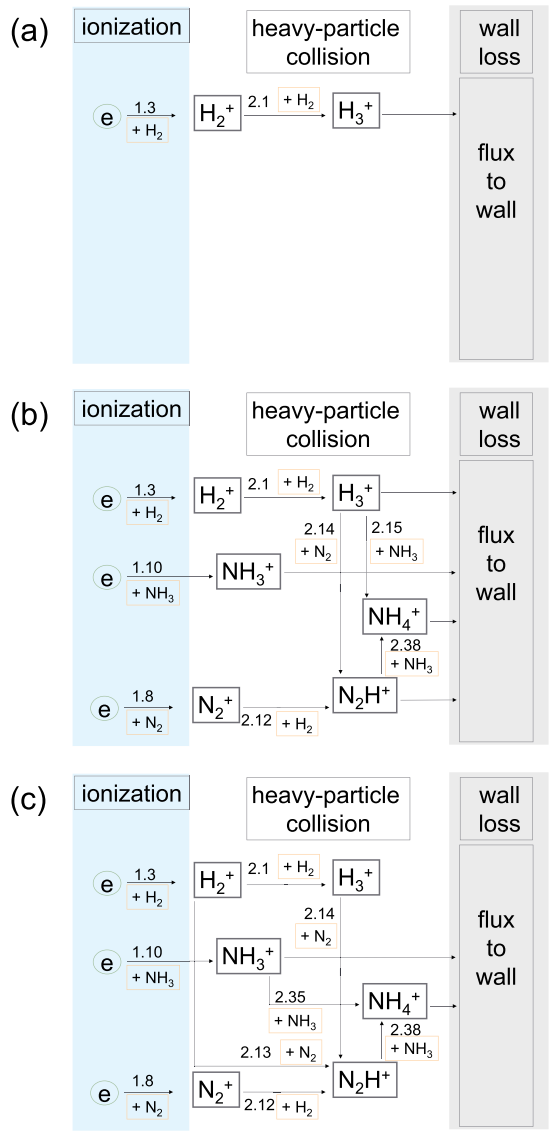

FIG. 9. Production and loss reactions of the most abundant ion species for $f_{N_2} = 0\%$ (a), $f_{N_2} = 7.9\%$ (b), and $f_{N_2} = 56\%$ (c). The numbers indicate the reactions outlined in Tables II and III.

A reaction is denoted as important if this reaction contributes at least 30% to the total production or total loss rate of the considered ion. For the sake of simplicity, the small Ar partial pressure fraction ($\approx 1.5\%$) in our plasma is not taken into account in the following discussion because the Ar^+ and ArH^+ ion densities are very low (percent range) and have only a small influence on the ion chemistry (see also Sec. VI C).

In the H_2 plasma ($f_{N_2} = 0\%$, Fig. 9(a)), H_3^+ is the dominant ion. The primary ion H_2^+ is produced by the electron-collision-induced reaction 1.3 ($e^- + H_2 \rightarrow H_2^+ + 2e^-$) through ionization of the background gas H_2. The secondary ion H_3^+ is solely produced by the ion-molecule reaction 2.1 ($H_2^+ + H_2 \rightarrow H_3^+ + H$). H_3^+ is mainly lost at the wall. The main loss channel of the primary ion H_2^+ is the conversion into H_3^+. Thus, the typical reaction chain of ions in an H_2 plasma is: electron-impact ionization of the background gas to produce primary ions, conversion of primary ions by ion-molecule reactions with the background gas species to produce secondary ions, and finally the flux of the secondary ions to the wall where they recombine and are lost from the plasma system.

As expected, by addition of N_2 to the H_2 plasma, the ion chemistry becomes more complex. However, in the H_2-N_2 plasma with low N_2 partial pressure fraction ($f_{N_2} = 7.9\%$, Fig. 9(b)), the basic reaction chain remains the same as in the H_2 plasma. At the beginning of the reaction chain is the ionization of the background gases H_2, N_2, and NH_3 for the production of primary ions H_2^+, N_2^+, and NH_3^+, respectively. The most abundant secondary ions are formed by proton transfer to a primary ion. However, the production of the secondary ions is significantly more complex than in pure H_2 plasma. H_3^+ is again generated predominantly from H_2^+ and lost at the wall. But, a small fraction of the H_3^+ ions are converted to NH_4^+ and N_2H^+. Although this is a minor loss channel for H_3^+, it is important for the production of NH_4^+ and N_2H^+. They are dominantly produced via reaction 2.15 ($H_3^+ + NH_3 \rightarrow NH_4^+ + H_2$) and via reaction 2.14 ($H_3^+ + N_2 \rightarrow N_2H^+ + H_2$), respectively, since the density of H_3^+ is very high. *A priori* one could anticipate that NH_4^+ and N_2H^+ would be produced from NH_3^+ by ion-molecule reactions via reaction 2.35 ($NH_3^+ + NH_3 \rightarrow NH_4^+ + NH_2$) and from N_2^+ via reaction 2.12 ($N_2^+ + H_2 \rightarrow N_2H^+ + H$), respectively, but according to the model, they are not. It is interesting to emphasize that the ion-molecule reaction 2.12 is now the dominant loss reaction for N_2^+ and not diffusion to the wall. In contrast, the main loss channel of the most abundant secondary ions (H_3^+, NH_4^+, and N_2H^+) and NH_3^+ is again the loss to the wall.

In contrast to H_2^+ and N_2^+, the primary ion NH_3^+ reaches the wall mostly without reactive collisions. The rate of reaction 2.35 which is the dominant loss channel of NH_3^+ in the plasma volume is given by the product of the densities of NH_3^+ and NH_3 and the corresponding rate coefficient $K_{2.35}$. While the values of $n_{NH_3^+}$ and $K_{2.35}$ are comparable with the corresponding values of the loss reactions for H_2^+ and N_2^+, the densities of H_2 and N_2 are much higher than that of NH_3. That is the reason why the rate for the ion-molecule reaction of NH_3^+ with NH_3 is much smaller than the dominant loss rates of H_2^+ and N_2^+. Furthermore, NH_3^+ hardly reacts with H_2 (see $K_{2.34}$ in Table III) and N_2.[66,90] Overall, the sum of the NH_3^+ loss rates of all volume reactions is less than the wall loss rate.

If the N_2 partial pressure fraction is increased even more, i.e., $f_{N_2} = 56\%$ (see Fig. 9(c)), the reaction chain (electron—primary ion—secondary ion—loss to wall) changes insofar that the secondary ions H_3^+ and N_2H^+ are not mainly lost by recombination at the wall, but by ion-molecule reactions in the plasma volume. These ion-molecule reactions of H_3^+ (reaction 2.14: $H_3^+ + N_2 \rightarrow N_2H^+ + H_2$) and N_2H^+ (reaction 2.38: $N_2H^+ + NH_3 \rightarrow NH_4^+ + N_2$) lead to the production of NH_4^+. The major loss channel of NH_4^+ is the loss to the wall. Due to the high N_2 density, H_2^+ is mainly transformed into N_2H^+ (reaction 2.13: $H_2^+ + N_2 \rightarrow N_2H^+ + H$). However, reaction 2.13 contributes only to a minor part to the total production of N_2H^+. N_2H^+ is predominantly produced by N_2^+ via reaction 2.12 ($N_2^+ + H_2 \rightarrow N_2H^+ + H$). Also for $f_{N_2} = 56\%$, NH_3^+ is mainly lost by recombination at

the wall. A smaller contribution to the loss of NH_3^+ provides reaction 2.35 ($NH_3^+ + NH_3 \rightarrow NH_4^+ + NH_2$).

The fact that the ion densities of NH_3^+ and NH_4^+ are larger than that of H_3^+ and N_2H^+ over a wide range of f_{N_2} can also be explained with the proton affinities E_{pa}. The values are for H_2 $E_{pa} = 4.37$ eV (taken from Ref. 91; corresponding ion H_3^+), N_2 5.12 eV (N_2H^+), NH_2 8.01 eV (NH_3^+), and NH_3 8.86 eV (NH_4^+). The sequence of proton affinities favors the production of NH_3^+ and NH_4^+ against H_3^+ and N_2H^+.

B. Discussion of the calculated radical densities

Because the radical densities were—with the exception of atomic H—not measured, the model results presented in Fig. 4 cannot directly be compared with the experimental data. However, we can assess the reliability of the calculated radical densities indirectly by a comparison of those modeled ion densities which are produced predominantly by direct ionization from the corresponding radicals. The latter will be discussed in the following for H, N, NH, and NH_2. First, we discuss here the correlation between radical densities and the resulting ion densities. As it was shown in a previous publication[23] for a H_2-Ar plasma at 1.0 Pa, H^+ is mainly produced by electron-induced ionization from H (reaction 1.2: $e^- + H \rightarrow H^+ + 2e^-$). This is also true for the H_2-N_2-Ar plasma where the fraction of reaction 1.2 on the total production rate is $R_{1.2}/R_{tot} \geq 67\%$ for all considered f_{N_2}. H^+ is mainly ($R_{wH^+}/R_{tot} \geq 53\%$) lost by recombination at the wall. NH^+ is primarily produced via reaction 1.17 ($e^- + NH \rightarrow NH^+ + 2e^-$). The contributions of reaction rate $R_{1.17}/R_{tot}$ to the total production rates at low and high N_2 partial pressure fraction are $R_{1.17}/R_{tot}(f_{N_2} = 0.8\%) = 61\%$ and $R_{1.17}/R_{tot}(f_{N_2} = 56\%) = 74\%$, respectively. NH^+ is lost predominantly via reaction 2.28 ($NH^+ + H_2 \rightarrow NH_2^+ + H$). N^+ is not significantly produced from atomic nitrogen but from other species: from N_2 via reaction 1.9 ($e^- + N_2 \rightarrow N^+ + N + 2e^-$), from N($D$) via reaction 4.10 ($e^- + N(D) \rightarrow N^+ + 2e^-$), and from NH via reaction 1.18 ($e^- + NH \rightarrow N^+ + H + 2e^-$). NH_2^+ is almost exclusively ($R_{1.11}/R_{tot} \geq 93\%$ for all considered f_{N_2}) produced from NH_3 via reaction 1.11 ($e^- + NH_3 \rightarrow NH_2^+ + H + 2e^-$). In conclusion, the densities of H and NH can be assessed by comparing with the corresponding ion densities. NH_2 plays for the formation of NH_2^+ almost no role.

It is important to keep in mind that two completely independent diagnostic methods were used to measure n_{H^+} (Fig. 7) and n_H (Fig. 4), namely, the PM and OES, respectively. The calculated density of the H^+ ions deviates to higher values and agrees only within an averaged factor of 3.5 with the experimentally determined H^+ ion density measured with the PM. Furthermore, the calculated atomic H density agrees within an averaged factor of 1.6 with values measured with OES (see Sec. V D). However, mass spectrometer measurements at mass channel 1 amu/e are rather difficult and error-prone so that the measured H^+ density should be considered with great care. We, therefore, have a higher confidence in the calculated ion density than in the one measured with the PM. Nevertheless, the measured ion density is in an acceptable agreement with the calculated ion density and can at least be considered as indication that the order of magnitude of the calculated H atom density is also reasonable. In the case of the H atom density, we have the additional OES data which are in good agreement with our model results. Finally, the calculated NH^+ ion density agrees satisfactorily with the measurement (see Fig. 8). The maximum deviation is a factor of 1.8. Since, as discussed above, NH^+ is mainly produced from NH, we take this reasonable agreement as a confirmation that the NH density is calculated realistically.

C. Variation of the Ar partial pressure

In Sec. VI A, we stated that in the H_2-N_2-Ar plasma with 1% Ar partial pressure fraction argon has only a small influence on the ion chemistry. To confirm this, the influence of Ar is investigated by a f_{Ar} variation between 0% and 56%. To keep the total pressure constant, for a fixed $f_{N_2} \approx 3\%$ under otherwise identical plasma conditions ($p = 1.5$ Pa and $P_{rf} = 200$ W) the H_2 partial pressure fraction was adjusted accordingly. The experimental and modeled results are shown in Figs. 10 and 11. It is worth mentioning that n_e increases by one order of magnitude, but n_{NH_3} increases only slightly by a factor of 1.5 when increasing f_{Ar} from 0% to 56%. T_e decreases from 3.9 eV ($f_{Ar} = 0\%$) to 3.1 eV ($f_{Ar} = 56\%$). At $f_{Ar} = 1\%$ and $f_{N_2} = 3\%$, NH_3^+ and NH_4^+ show the highest ion densities, followed by N_2H^+. n_{ArH^+} and n_{Ar^+} are one and two orders of magnitude below $n_{NH_3^+}$, respectively. For an increase in Ar partial pressure fraction from 1% to 10%, n_{ArH^+} and n_{Ar^+} increase by one order of magnitude, while all other ion densities remain approximately constant. This confirms our statement from Sec. VI A. For larger partial pressure fraction, the ion chemistry is influenced. In the range of $30\% < f_{Ar} < 60\%$, NH_3^+ and ArH^+ are dominant. The agreement between calculated ion densities and experimental values is essentially the same as already discussed for the N_2 variation. ArH^+ is formed primarily from Ar^+ via reaction 2.6 ($Ar^+ + H_2 \rightarrow ArH^+ + H$). NH_3^+ is produced via reaction 1.10 ($e^- + NH_3 \rightarrow NH_3^+ + 2e^-$) and 2.39 ($Ar^+ + NH_3 \rightarrow NH_3^+ + Ar$). At $f_{Ar} = 56\%$, the ion chemistry is significantly influenced by ArH^+: While for lower Ar,

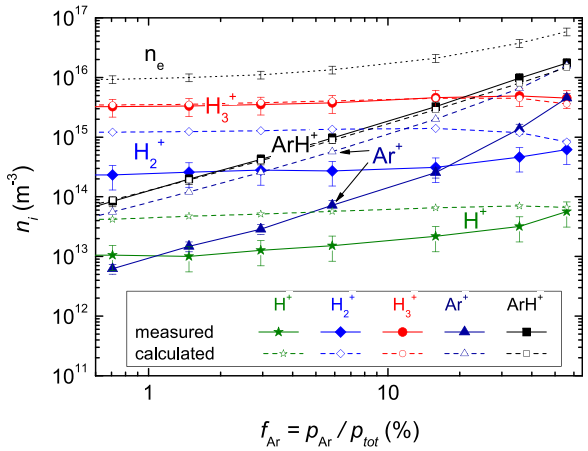

FIG. 10. Measured and calculated ion densities n_i of H_x^+ ($x = 1 - 3$), Ar^+, and ArH^+ as well as n_e as a function of f_{Ar}.

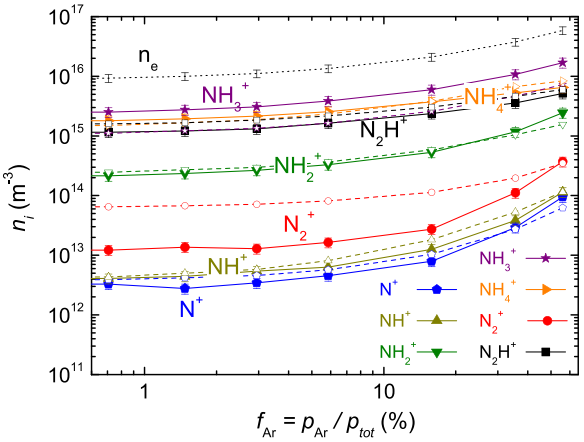

FIG. 11. Measured (solid symbols) and calculated (open symbols) ion densities n_i of NH_x^+ ($x = 0-4$), N_2^+, and N_2H^+ as well as n_e as a function of f_{Ar}.

partial pressure fractions NH_4^+ and N_2H^+ are produced by H_3^+ (see Fig. 9), for $f_{Ar} = 56\%$ these ions are produced mainly from ArH^+.

D. Comparison with a DC plasma

Carrasco *et al.*[3,28] studied H_2-N_2 low-pressure plasmas which are comparable to some extent to the here-investigated H_2-N_2-Ar plasma. They used a hollow cathode DC discharge in a cylindrical-shaped stainless steel plasma chamber with a chamber volume comparable to our setup. They measured the densities of neutral and ion species and compared their results with a rate equation model. In Ref. 3, they investigated several pressures at a fixed N_2 partial pressure fraction of 10% (P_{off}) and in Ref. 28 a f_{N_2} variation at a constant pressure of 8 Pa. They applied sheath voltages of 300–450 eV with corresponding sheath thicknesses in the range of 15–20 mm. During P_{on}, the N_2 partial pressure fraction measured with a quadrupole mass spectrometer was $f_{N_2} \approx 7\%$. It was independent of the investigated pressure within the experimental uncertainty. f_{NH_3} decreased from 5% at 0.8 Pa via 3% at 2 Pa to 2.5% at 8 Pa. For comparison, the results in this work are $f_{NH_3} = 5.7\%$ at $f_{N_2} = 7.9\%$ and $p = 1.5$ Pa. They measured an electron temperature and density of $T_e = (3.4 \pm 0.5)$ eV and $n_e = (3.5 \pm 0.5) \times 10^{16}$ m^{-3}, respectively, for $p = 2$ Pa and $f_{N_2} = 7\%$. For comparison, in the present work at $p = 1.5$ Pa and $f_{N_2} = 7.9\%$ T_e and n_e are (3.5 ± 0.4) eV and $(1.3 \pm 0.2) \times 10^{16}$ m^{-3}, respectively. In view of the very different plasma generation type and the different plasma chamber geometries between the present work and Carrasco *et al.*, we consider this a fairly good agreement. Thus, it is meaningful to compare the relative ion densities of the two considered studies with each other.

Carrasco *et al.*[3] calculated the densities of the ions and the radicals with a rate equation model comparable to the model applied in this work. Comparing the rate coefficients K_k with $k = 1.3$, 1.6, 1.8–1.11, 1.15–1.18 for electron-induced collisions presented in Table II to data from Carrasco *et al.*[3] in the T_e range from 3 to 7 eV we find an agreement within 30%, whereas other K_k from Table II deviate more than 30%.[54] The rate coefficients for the ion-molecule reactions agree between Carrasco *et al.* and the present work since both used values provided by Anicich.[66] Carrasco *et al.* used the ion wall loss rate coefficient K_{wi} as fit parameter to fulfill the quasi-neutrality condition. In contrast, in the present study K_{wi} is obtained by a sheath model, but T_e is used as fit parameter to fulfill the quasi-neutrality condition.

Carrasco *et al.*[3] measured the relative ion densities with a plasma monitor (plasma process monitor PPM 422), which is comparable to the instrument used in this work. For the relative ion concentration, they integrated the measured ion energy distributions and multiplied the value by a mass transmission factor T_{md}. They obtained experimentally[3] a $T_{md} \propto (M_i)^{-1/2}$ (M_i—ion mass), which is in agreement with the present study.

In a H_2-N_2 plasma investigated in Refs. 3 and 28, two parameter variations were investigated: on the one hand, different pressures (0.8, 2 and 8 Pa)[3] at a fixed N_2 partial pressure fraction of $f_{N_2} = 7\%$ and, on the other hand, different N_2 partial pressure fractions ($0 < f_{N_2} < 10\%$)[28] at a fixed pressure of $p = 8$ Pa. At $f_{N_2} = 7\%$ and 0.8 Pa, they found that both model and experiment result in similar ion densities for H_2^+, H_3^+, NH_3^+, NH_4^+, and N_2H^+. For increasing pressure, the NH_4^+ density increased and showed at 8 Pa the by far highest ion density.[3] Furthermore, Carrasco *et al.* reported that NH_3^+ is predominantly lost by recombination at the wall. This is also confirmed in the present work. In Ref. 28, Carrasco *et al.* examined a H_2 plasma at 8 Pa with small N_2 admixture. They observed that for $0 < f_{N_2} < 10\%$ the secondary ions H_3^+, NH_4^+, and N_2H^+ have the highest ion densities and that correspondingly the primary ions H_2^+ and N_2^+ contribute only a very small fraction to the total ion density. While in the H_2 plasma with low N_2 partial pressure fraction ($f_{N_2} < 2\%$) H_3^+ is the dominant ion,[28] NH_4^+ becomes dominant at increasing f_{N_2} ($f_{N_2} > 4\%$).[28] Also in the present work at 1.5 Pa and $f_{N_2} < 3\%$, H_3^+ is the dominant ion species which is in accordance with Carrasco *et al.*[28] In the present work at $f_{N_2} > 3\%$, the ion densities of NH_3^+ and NH_4^+ are most abundant and have approximately the same values. It is important to note that a pressure of 8 Pa was used which causes a significant increase of $n_{NH_4^+}$ by charge exchange reactions compared to $n_{NH_3^+}$.

Furthermore, it is interesting to note that Carrasco *et al.*[28] also show modeling results for the time evolution of the ion species H_3^+, NH_3^+, NH_4^+, and N_2H^+ and the background gas densities after plasma ignition. For times t lower than 0.1 s the NH_3 density is of the order of the N_2 density since NH_3 is produced slowly by a number of reaction steps occurring at the wall. $n_{H_3^+}$ shows a maximum at $t \approx 10^{-7}$ s (dominant ion), decreases further, and for $t \gtrsim 10^{-6}$ s H_3^+ is replaced by N_2H^+ as the dominant ion. Only for $t \gtrsim 3 \times 10^{-1}$ s, NH_4^+ (produced by ion-molecule collisions with NH_3, i.e., reactions 2.15, 2.35, and 2.38) becomes the dominant ion species because the production of ammonia occurring at the chamber wall ($t \approx 0.1$ s) is several orders of magnitudes slower than ionization processes ($t \approx 10^{-7}$ s). These results have clearly shown that NH_4^+ cannot be formed without NH_3 being present, which is in agreement with the result of the present rate equation model. In summary, the observations and discussions with respect to the ion densities and ion

chemistry of H_3^+, NH_3^+, NH_4^+, and N_2H^+ between Carrasco *et al*. and the present work are essentially in agreement.

VII. SUMMARY

Inductively coupled H_2-N_2-Ar plasmas were extensively studied at a pressure of 1.5 Pa and a *rf* power of 200 W. The N_2 partial pressure fraction was increased from $f_{N_2} = 0\%$ to 56% by simultaneous reduction of the H_2 partial pressure fraction. The Ar partial pressure fraction was constant at about 1%. In the H_2-N_2-Ar plasma, the stable species NH_3 is produced and contributes up to 12% to the background gas. In the studied plasma, NH_3 is almost exclusively produced on the surfaces of the chamber walls. The experimentally determined ion (n_i) and radical (n_{rad}) densities were compared to the results of a rate equation model.

To calculate the radical densities with the rate equation model, it is necessary to know the corresponding wall loss times t_{wrad} for the radical species. t_{wrad} was determined experimentally by the decay of radical densities in the temporal afterglow of pulsed plasmas. With this the absolute densities of the radical species were calculated with the rate equation model.

The measurements with the plasma monitor show that H_3^+ is the dominant ion in the range of $0.0 \leq f_{N_2} < 3.4\%$. For $3.4 < f_{N_2} < 40\%$, NH_3^+ and NH_4^+ have the highest densities and their densities agree within the experimental uncertainty. For $f_{N_2} = 56\%$, N_2H^+ is the dominant ion and NH_3^+ and NH_4^+ have a slightly lower density. These four most abundant ion species contribute more than 90% to the total ion density $n_{i,tot}$ for all considered f_{N_2}. Ion species with densities in the range between 0.5% and 10% of $n_{i,tot}$ are H_2^+, ArH^+, and NH_2^+. Ion species with densities less than 0.5% of $n_{i,tot}$ are H^+, Ar^+, N^+, and NH^+.

The applied rate equation model describes the measured ion densities of the H_2-N_2-Ar plasmas reasonably well. The main features, i.e., the qualitative abundance of the ion species and the dependence of the ion density on the N_2 partial pressure fraction as well as the electron temperature, are well reproduced by the model. Nevertheless, some quantitative deviations between model and experiment remain. The main discrepancy is that the modeled densities of the primary ions H_2^+, N_2^+, and Ar^+ are clearly higher than the measured values.

Overall, a comprehensive investigation of inductively coupled H_2-N_2-Ar plasmas was carried out, which results in the experimental determination of absolute ion and radical densities. Furthermore, the densities were calculated using a zero-dimensional model, which adequately describes the main features of the measured densities. The model allows to identify the most important plasma-chemical reactions in the investigated H_2-N_2-Ar plasma.

ACKNOWLEDGMENTS

We gratefully acknowledge help from T. Dürbeck and W. Hohlenburger for technical assistance.

[1]S. Xu, S. Y. Huang, I. Levchenko, H. P. Zhou, D. Y. Wei, S. Q. Xiao, L. X. Xu, W. S. Yan, and K. Ostrikov, "Highly efficient silicon nanoarray solar cells by a single-step plasma-based process," Adv. Energy Mater. **1**, 373–376 (2011).
[2]K. Ostrikov, U. Cvelbar, and A. B. Murphy, "Plasma nanoscience: Setting directions, tackling grand challenges," J. Phys. D: Appl. Phys. **44**, 174001 (2011).
[3]E. Carrasco, M. Jimenez-Redondo, I. Tanarro, and V. J. Herrero, "Neutral and ion chemistry in low pressure dc plasmas of H_2/N_2 mixtures: Routes for the efficient production of NH_3 and NH_4^+," Phys. Chem. Chem. Phys. **13**, 19561–19572 (2011).
[4]T.-P. Ma, "Making silicon nitride film a viable gate dielectric," IEEE Trans. Electron Devices **45**, 680–690 (1998).
[5]A. G. Aberle, "Overview on SiN surface passivation of crystalline silicon solar cells," in *PVSEC* [Sol. Energy Mater. Sol. Cells **65**, 239–248 (2001)].
[6]H. Nagai, S. Takashima, M. Hiramatsu, M. Hori, and T. Goto, "Behavior of atomic radicals and their effects on organic low dielectric constant film etching in high density N_2/H_2 and N_2/NH_3 plasmas," J. Appl. Phys. **91**, 2615–2621 (2002).
[7]C. S. Moon, K. Takeda, S. Takashima, M. Sekine, Y. Setsuhara, M. Shiratani, and M. Hori, "Surface loss probabilities of H and N radicals on different materials in afterglow plasmas employing H_2 and N_2 mixture gases," J. Appl. Phys. **107**, 103310 (2010).
[8]J. H. van Helden, P. J. van den Oever, W. M. M. Kessels, M. C. M. van de Sanden, D. C. Schram, and R. Engeln, "Production mechanisms of NH and NH_2 radicals in N_2-H_2 plasmas," J. Phys. Chem. A **111**, 11460–11472 (2007).
[9]A. Ricard, B. F. Gordiets, M. J. Pinheiro, C. M. Ferreira, G. Baravian, J. Amorim, S. Bockel, and H. Michel, "Diagnostic and modeling of N_2-H_2 discharges for iron nitriding," Eur. Phys. J.: Appl. Phys. **4**, 87–93 (1998).
[10]H. Kim, "Atomic layer deposition of metal and nitride thin films: Current research efforts and applications for semiconductor device processing," J. Vac. Sci. Technol., B **21**, 2231–2261 (2003).
[11]K. V. Laer, S. Tinck, V. Samara, J. F. de Marneffe, and A. Bogaerts, "Etching of low-k materials for microelectronics applications by means of a N_2/H_2 plasma: Modeling and experimental investigation," Plasma Sources Sci. Technol. **22**, 025011 (2013).
[12]E. N. Eremin, Russ. J. Phys. Chem. **49**, 1112 (1975).
[13]P. Vankan, T. Rutten, S. Mazouffre, D. C. Schram, and R. Engeln, "Absolute density measurements of ammonia produced via plasma-activated catalysis," Appl. Phys. Lett. **81**, 418–420 (2002).
[14]D. Neuwirth, V. Rohde, T. Schwarz-Selinger, and A. U. G. Team, "Formation of ammonia during nitrogen-seeded discharges at ASDEX Upgrade," Plasma Phys. Controlled Fusion **54**, 085008 (2012).
[15]M. Oberkofler, D. Douai, S. Brezinsek, J. Coenen, T. Dittmar, A. Drenik, S. Romanelli, E. Joffrin, K. McCormick, M. Brix, G. Calabro, M. Clever, C. Giroud, U. Kruezi, K. Lawson, C. Linsmeier, A. M. Rojo, A. Meigs, S. Marsen, R. Neu, M. Reinelt, B. Sieglin, G. Sips, M. Stamp, and F. Tabares, "First nitrogen-seeding experiments in JET with the ITER-like wall," in *Proceedings of the 20th International Conference on Plasma-Surface Interactions in Controlled Fusion Devices* [J. Nucl. Mater. **438**(Suppl.), S258–S261 (2013)].
[16]A. Kallenbach, R. Dux, J. C. Fuchs, R. Fischer, B. Geiger, L. Giannone, A. Herrmann, T. Lunt, V. Mertens, R. McDermott, R. Neu, T. Puetterich, S. Rathgeber, V. Rohde, K. Schmid, J. Schweinzer, W. Treutterer, and A. U. G. Team, "Divertor power load feedback with nitrogen seeding in ASDEX Upgrade," Plasma Phys. Controlled Fusion **52**, 055002 (2010).
[17]A. Kallenbach, M. Balden, R. Dux, T. Eich, C. Giroud, A. Huber, G. Maddison, M. Mayer, K. McCormick, R. Neu, T. Petrie, T. Pütterich, J. Rapp, M. Reinke, K. Schmid, J. Schweinzer, and S. Wolfe, "Plasma surface interactions in impurity seeded plasmas," in *Proceedings of the 19th International Conference on Plasma-Surface Interactions in Controlled Fusion* [J. Nucl. Mater. **415**, S19–S26 (2011)].
[18]A. Kallenbach, M. Bernert, T. Eich, J. Fuchs, L. Giannone, A. Herrmann, J. Schweinzer, W. Treutterer, and A. U. G. Team, "Optimized tokamak power exhaust with double radiative feedback in ASDEX Upgrade," Nucl. Fusion **52**, 122003 (2012).
[19]G. Maddison, C. Giroud, B. Alper, G. Arnoux, I. Balboa, M. N. A. Beurskens, A. Boboc, S. Brezinsek, M. Brix, M. Clever, R. Coelho, J. W. Coenen, I. Coffey, P. C. da Silva Aresta Belo, S. Devaux, P. Devynck, T. Eich, R. C. Felton, J. Flanagan, L. Frassinetti, L. Garzotti, M. Groth, S. Jachmich, A. Järvinen, E. Joffrin, M. A. H. Kempenaars, U. Kruezi, K. D. Lawson, M. Lehnen, M. J. Leyland, Y. Liu, P. Lomas, C. G. Lowry,

S. Marsen, G. F. Matthews, G. K. McCormick, A. G. Meigs, A. W. Morris, R. Neu, I. Nunes, M. Oberkofler, F. G. Rimini, S. Saarelma, B. Sieglin, A. C. C. Sips, A. Sirinelli, M. F. Stamp, G. J. van Rooij, D. J. Ward, M. Wischmeier, and J. E. T. E. F. D. A. Contributors, "Contrasting H-mode behaviour with deuterium fuelling and nitrogen seeding in the all-carbon and metallic versions of JET," Nucl. Fusion **54**, 073016 (2014).
[20]J. L. Jauberteau, I. Jauberteau, and J. Aubreton, "NH_3 and $NH_{x<3}$ radicals synthesis downstream a microwave discharge sustained in an Ar-N_2-H_2 gas mixture. Study of surface reactive processes and determination of rate constants," J. Phys. D: Appl. Phys. **35**, 665 (2002).
[21]I. Jauberteau, J. L. Jauberteau, M. N. Séméria, A. Larré, J. Piaguet, and J. Aubreton, "Plasma nitriding of thin molybdenum layers at low temperature," Surf. Coat. Technol. **116–119**, 222–228 (1999).
[22]M. Sode, T. Schwarz-Selinger, and W. Jacob, "Quantitative determination of mass-resolved ion densities in H_2-Ar inductively coupled radio frequency plasmas," J. Appl. Phys. **113**, 093304 (2013).
[23]M. Sode, T. Schwarz-Selinger, and W. Jacob, "Ion chemistry in H_2-Ar low temperature plasmas," J. Appl. Phys. **114**, 063302 (2013).
[24]N. Fox-Lyon and G. S. Oehrlein, "Isotope effects on plasma species of Ar/H_2/D_2 plasmas," J. Vac. Sci. Technol., B **32**, 041206 (2014).
[25]M. Jimenez-Redondo, M. Cueto, J. L. Domenech, I. Tanarro, and V. J. Herrero, "Ion kinetics in Ar/H_2 cold plasmas: the relevance of ArH^+," RSC Adv. **4**, 62030–62041 (2014).
[26]R. A. Arakoni, A. N. Bhoj, and M. J. Kushner, "H_2 generation in Ar/NH_3 microdischarges," J. Phys. D: Appl. Phys. **40**, 2476 (2007).
[27]E. Carrasco, V. J. Herrero, and I. Tanarro, "Time-resolved diagnostics and kinetic modelling of the ignition transient of a H_2 + 0.1 N_2 square wave modulated hollow cathode discharge," J. Phys. D: Appl. Phys. **45**, 305201 (2012).
[28]E. Carrasco, I. Tanarro, V. J. Herrero, and J. Cernicharo, "Proton transfer chains in cold plasmas of H_2 with small amounts of N_2. the prevalence of NH_4^+," Phys. Chem. Chem. Phys. **15**, 1699–1706 (2013).
[29]S. Jang and W. Lee, "Pressure and input power dependence of Ar/N_2H_2 inductively coupled plasma systems," J. Vac. Sci. Technol., A **19**, 2335 (2001).
[30]J. H. van Helden, W. Wagemans, G. Yagci, R. A. B. Zijlmans, D. C. Schram, R. Engeln, G. Lombardi, G. D. Stancu, and J. Röpcke, "Detailed study of the plasma-activated catalytic generation of ammonia in N_2-H_2 plasmas," J. Appl. Phys. **101**, 043305 (2007).
[31]S. J. Kang and V. M. Donnelly, "Optical absorption and emission spectroscopy studies of ammonia-containing plasmas," Plasma Sources Sci. Technol. **16**, 265 (2007).
[32]S. Chen, H. Kondo, K. Ishikawa, K. Takeda, M. Sekine, H. Kano, S. Den, and M. Hori, "Behaviors of absolute densities of N, H, and NH_3 at remote region of high-density radical source employing N_2–H_2 mixture plasmas," Jpn. J. Appl. Phys., Part 1 **50**, 01AE03 (2011).
[33]I. Burlacov, K. Börner, H.-J. Spies, H. Biermann, D. Lopatik, H. Zimmermann, and J. Röpcke, "In-situ monitoring of plasma enhanced nitriding processes using infrared absorption and mass spectroscopy," Surf. Coat. Technol. **206**, 3955–3960 (2012).
[34]C. S. Moon, K. Takeda, S. Takashima, M. Sekine, Y. Setsuhara, M. Shiratani, and M. Hori, "High performance of compact radical monitoring probe in H_2/N_2 mixture plasma," J. Vac. Sci. Technol., B **28**, L17–L20 (2010).
[35]S. Touimi, J. L. Jauberteau, I. Jauberteau, and J. Aubreton, "Plasma chemistry and diagnostic in an Ar-N_2-H_2 microwave expanding plasma used for nitriding treatments," J. Phys. D: Appl. Phys. **43**, 205203 (2010).
[36]S. Peter, R. Pintaske, G. Hecht, and F. Richter, "Determination of mass and energy distribution of ions in glow discharges," Surf. Coat. Technol. **59**, 97–100 (1993).
[37]B. Gordiets, C. M. Ferreira, M. J. Pinheiro, and A. Ricard, "Self-consistent kinetic model of low-pressure N_2-H_2 flowing discharges: I. Volume processes," Plasma Sources Sci. Technol. **7**, 363 (1998).
[38]B. Gordiets, C. M. Ferreira, M. J. Pinheiro, and A. Ricard, "Self-consistent kinetic model of low-pressure N_2-H_2 flowing discharges: II. Surface processes and densities of N, H, NH_3 species," Plasma Sources Sci. Technol. **7**, 379 (1998).
[39]E. Tatarova, F. M. Dias, B. Gordiets, and C. M. Ferreira, "Molecular dissociation in N_2-H_2 microwave discharges," Plasma Sources Sci. Technol. **14**, 19 (2005).
[40]A. Garscadden and R. Nagpal, "Non-equilibrium electronic and vibrational kinetics in H_2-N_2 and H_2 discharges," Plasma Sources Sci. Technol. **4**, 268 (1995).
[41]V. A. Kadetov, "Diagnostics and modeling of an inductively coupled radio frequency discharge in hydrogen," Ph.D. thesis (Ruhr Universität Bochum, 2004).
[42]W. Walcher, "Über eine Ionenequelle für massenspektroskopische Isotopentrennung," Z. Phys. **122**, 62–85 (1944).
[43]M. Sode, T. Schwarz-Selinger, W. Jacob, and H. Kersten, "Wall loss of atomic nitrogen determined by ionization threshold mass spectrometry," J. Appl. Phys. **116**, 193302 (2014).
[44]M. Sode, T. Schwarz-Selinger, W. Jacob, and H. Kersten, "Surface loss probability of atomic hydrogen for different electrode cover materials investigated in H_2-Ar low-pressure plasmas," J. Appl. Phys. **116**, 013302 (2014).
[45]S. V. Dudin, A. P. Jatskov, and V. I. Farenik, Tekhnol. Konstr. Elektron. Appar. **3**, 43 (2002).
[46]P. McNeely, S. Dudin, S. Christ-Koch, and U. Fantz, "A Langmuir probe system for high power RF-driven negative ion sources on high potential," Plasma Sources Sci. Technol. **18**, 014011 (2009).
[47]H. Singh, J. W. Coburn, and D. B. Graves, "Appearance potential mass spectrometry: Discrimination of dissociative ionization products," J. Vac. Sci. Technol., A **18**, 299 (2000).
[48]S. Matsuda, H. Shimosato, M. Yumoto, and T. Sakai, "Detection of nitrogen metastable molecules by using the threshold ionization mass spectrometry," Electr. Eng. Jpn. **147**, 17–24 (2004).
[49]H. Singh, J. W. Coburn, and D. B. Graves, "Recombination coefficients of O and N radicals on stainless steel," J. Appl. Phys. **88**, 3748–3755 (2000).
[50]P. Kae-Nune, J. Perrin, J. Jolly, and J. Guillon, "Surface recombination probabilities of H on stainless steel, a-Si:H and oxidized silicon determined by threshold ionization mass spectrometry in H_2 RF discharges," Surf. Sci. Lett. **360**, L495 (1996).
[51]M. Bauer, T. Schwarz-Selinger, W. Jacob, and A. v. Keudell, "Growth precursor for a–C:H film deposition in pulsed inductively coupled methane plasmas control of the plasma chemistry of a pulsed inductively coupled methane plasma," J. Appl. Phys. **98**, 073302 (2005).
[52]T. Schwarz-Selinger, V. Dose, W. Jacob, and A. von Keudell, "Quantification of a radical beam source for methyl radicals," J. Vac. Sci. Technol., A **19**, 101 (2001).
[53]S. Agarwal, B. Hoex, M. C. M. van de Sanden, D. Maroudas, and E. S. Aydil, "Absolute densities of N and excited N_2 in a N_2 plasma," Appl. Phys. Lett. **83**, 4918–4920 (2003).
[54]M. Sode, "Quantitative Beschreibung von Wasserstoff-Stickstoff-Argon-Mischplasmen," Ph.D. thesis (Universität Kiel, 2013) (in German). Available at http://d-nb.info/1048558398
[55]A. Sandu and R. Sanders, see http://people.cs.vt.edu/asandu/Software/Kpp/ for *KPP—The Kinetic Preprocessor, Version 2.2.1*, 2006.
[56]V. Damian, A. Sandu, M. Damian, F. Potra, and G. R. Carmichael, "The kinetic preprocessor KPP–A software environment for solving chemical kinetics," Comput. Chem. Eng. **26**, 1567–1579 (2002).
[57]T. Kimura and H. Kasugai, "Properties of inductively coupled rf Ar/H_2 plasmas: Experiment and global model," J. Appl. Phys. **107**, 083308 (2010).
[58]J.-S. Yoon, M.-Y. Song, J.-M. Han, S. H. Hwang, W.-S. Chang, B. Lee, and Y. Itikawa, "Cross sections for electron collisions with hydrogen molecules," J. Phys. Chem. Ref. Data **37**, 913–931 (2008).
[59]M. B. Shah, D. S. Elliott, and H. B. Gilbody, "Pulsed crossed-beam study of the ionisation of atomic hydrogen by electron impact," J. Phys. B: Atom. Mol. Phys. **20**, 3501–3514 (1987).
[60]R. C. Wetzel, F. A. Baiocchi, T. R. Hayes, and R. S. Freund, "Absolute cross sections for electron-impact ionization of the rare-gas atoms by the fast-neutral-beam method," Phys. Rev. A **35**, 559–577 (1987).
[61]Y. Itikawa, "Cross sections for electron collisions with nitrogen molecules," J. Phys. Chem. Ref. Data **35**, 31–53 (2006).
[62]Y.-K. Kim and J.-P. Desclaux, "Ionization of carbon, nitrogen, and oxygen by electron impact," Phys. Rev. A **66**, 012708 (2002).
[63]V. Tarnovsky, H. Deutsch, and K. Becker, "Cross-sections for the electron impact ionization of ND_x (x =1-3)," Int. J. Mass Spectrom. Ion Processes **167/168**, 69–78 (1997).
[64]T. D. Märk, F. Egger, and M. Cheret, "Ionization of ammonia and deuterated ammonia by electron impact from threshold up to 180 eV," J. Chem. Phys. **67**, 3795–3802 (1977).
[65]M. Yousfi and M. D. Benabdessadok, "Boltzmann equation analysis of electron-molecule collision cross sections in water vapor and ammonia," J. Appl. Phys. **80**, 6619–6630 (1996).
[66]V. K. Anicich, "Evaluated bimolecular ion-molecule gas phase kinetics of positive ions for use in modelling planetary atmospheres, cometary comae, and interstellar clouds," J. Phys. Chem. Ref. Data **22**, 1469–1569 (1993).

[67]K. Tao, D. Mao, and J. Hopwood, "Ionized physical vapor deposition of titanium nitride: A global plasma model," J. Appl. Phys. **91**, 4040–4048 (2002).
[68]M. A. Lieberman and A. J. Lichtenberg, *Principles of Plasma Discharges and Materials Processing* (John Wiley and Sons, Inc., Hoboken, New Jersey, 2005).
[69]V. A. Godyak, *Soviet Radio Frequency Discharge Research* (Delphic Associates, Falls Church, VA, 1986).
[70]A. Bogaerts and R. Gijbels, "Hybrid Monte Carlo—fluid modeling network for an argon/hydrogen direct current glow discharge," Spectrochim. Acta, Part B **57**, 1071–1099 (2002).
[71]A. V. Phelps, "Cross sections and swarm coefficients for nitrogen ions and neutrals in N_2 and argon ions and neutrals in Ar for energies from 0.1 eV to 10 KeV," J. Phys. Chem. Ref. Data **20**, 557 (1991).
[72]V. Voitsenya, S. Masuzaki, O. Motojima, and A. Sagara, "Impact of N_2-H_2 mixture plasma on carbon-containing film," Probl. At. Sci. Technol., Ser.: Plasma Phys. **2006**, 141–143.
[73]V. Voitsenya, S. Masuzaki, O. Motojima, and A. Sagara, "Impact of N_2-H_2 mixture plasma on carbon-containing film" (unpublished 2006).
[74]M. T. Bowers and D. D. Elleman, "Kinetic analysis of the concurrent ion–-molecule reactions in mixtures of argon and nitrogen with H_2, D_2, and HD utilizing ion-ejection–ion-cyclotron-resonance techniques," J. Chem. Phys. **51**, 4606–4617 (1969).
[75]A. T. Hjartarson, E. G. Thorsteinsson, and J. T. Gudmundsson, "Low pressure hydrogen discharges diluted with argon explored using a global model," Plasma Sources Sci. Technol. **19**, 065008 (2010).
[76]T. Kimura and H. Kasugai, "Experiments and global model of inductively coupled rf Ar/N_2 discharges," J. Appl. Phys. **108**, 033305 (2010).
[77]E. G. Thorsteinsson and J. T. Gudmundsson, "A global (volume averaged) model of a nitrogen discharge: I. steady state," Plasma Sources Sci. Technol. **18**, 045001 (2009).
[78]M. Gerl, "Modellierung von Teilchendichten in Stickstoff-Niedertemperaturplasmen," Bachelor thesis (Technische Universität München, 2011) (in German).
[79]P. J. Chantry, "A simple formula for diffusion calculations involving wall reflection and low density," J. Appl. Phys. **62**, 1141–1148 (1987).
[80]S. Takashima, M. Hori, T. Goto, A. Kono, and K. Yoneda, "Absolute concentration and loss kinetics of hydrogen atom in methane and hydrogen plasmas," J. Appl. Phys. **90**, 5497–5503 (2001).
[81]J. Jolly and J.-P. Booth, "Atomic hydrogen densities in capacitively coupled very high-frequency plasmas in H_2: Effect of excitation frequency," J. Appl. Phys. **97**, 103305 (2005).
[82]A. Rousseau, G. Cartry, and X. Duten, "Surface recombination of hydrogen atoms studied by a pulsed plasma excitation technique," J. Appl. Phys. **89**, 2074–2078 (2001).
[83]K. Kutasi and J. Loureiro, "Role of the wall reactor material on the species density distributions in an N_2 O_2 post-discharge for plasma sterilization," J. Phys. D **40**, 5612 (2007).
[84]U. Cvelbar, M. Mozetič, I. Poberaj, D. Babič, and A. Ricard, "Characterization of hydrogen plasma with a fiber optics catalytic probe," Thin Solid Films **475**, 12–16 (2005).
[85]F. Gaboriau, U. Cvelbar, M. Mozetič, A. Erradi, and B. Rouffet, "Comparison of TALIF and catalytic probes for the determination of nitrogen atom density in a nitrogen plasma afterglow," J. Phys. D: Appl. Phys. **42**, 055204 (2009).
[86]A. D. Tserepi and T. A. Miller, "Two-photon absorption laser-induced fluorescence of H atoms: A probe for heterogeneous processes in hydrogen plasmas," J. Appl. Phys. **75**, 7231–7236 (1994).
[87]S. F. Adams and T. A. Miller, "Surface and volume loss of atomic nitrogen in a parallel plate rf discharge reactor," Plasma Sources Sci. Technol. **9**, 248 (2000).
[88]M. Osiac, T. Schwarz-Selinger, D. O'Connell, B. Heil, Z. L. Petrovic, M. M. Turner, T. Gans, and U. Czarnetzki, "Plasma boundary sheath in the afterglow of a pulsed inductively coupled RF plasma," Plasma Sources Sci. Technol. **16**, 355–363 (2007).
[89]W. Poschenrieder, private communication, 2012.
[90]N. G. Adams, D. Smith, and J. F. Paulson, "An experimental survey of the reactions of NH_n^+ ions ($n = 0$ to 4) with several diatomic and polyatomic molecules at 300 K," J. Chem. Phys. **72**, 288–297 (1980).
[91]E. P. L. Hunter and S. G. Lias, "Evaluated gas phase basicities and proton affinities of molecules: An update," J. Phys. Chem. Ref. Data **27**, 413 (1998).